RSC Advances

PAPER

View Article Online
View Journal | View Issue

Cite this: *RSC Adv.*, 2026, **16**, 27915

Chalcone–sulfonate ester derivatives as dual urease and α-amylase inhibitors: synthesis, biological evaluation and integrated computational studies

Zobia Noreen,[a] Amina Sadiq,*[a] Nafeesa Naeem,[b] Usama Raza,[c] Ishtiaq Ahmed,[d] Samar Y. Al Nami,[e] Aisha Hossan,[e] Magdi E. A. Zaki[f] and Ehsan Ullah Mughal *[b]

A series of chalcone–sulfonate ester derivatives (**1–7**) were synthesized and evaluated for their potential inhibitory activity against urease and α-amylase enzymes. The chemical structures of the synthesized compounds were confirmed using appropriate spectroscopic techniques (IR, NMR and mass spectrometry). The biological potential of these derivatives was assessed through *in vitro* enzyme inhibition assays, where several compounds demonstrated promising activity against both urease and α-amylase, suggesting their possible application in the management of urease-related infections and disorders associated with carbohydrate metabolism. Structure–activity relationship (SAR) analysis revealed that the nature and position of substituents on the aromatic rings significantly influenced the inhibitory potency of the compounds. To further understand the interaction mechanisms, molecular docking studies were performed to investigate the binding modes of the synthesized molecules within the active sites of the target enzymes. In addition, pharmacokinetic properties were evaluated through *in silico* ADME analysis to assess drug-likeness and potential bioavailability. Furthermore, molecular dynamics (MD) simulations were carried out to examine the stability and dynamic behaviour of the ligand–enzyme complexes, while density functional theory (DFT) calculations were employed to explore the electronic characteristics and reactivity parameters of the compounds. The integrated experimental and computational findings highlight the potential of chalcone–sulfonate esters as promising scaffolds for the development of novel urease and α-amylase inhibitors.

Received 29th March 2026
Accepted 12th May 2026

DOI: 10.1039/d6ra02588a

rsc.li/rsc-advances

1. Introduction

Chalcones represent an important class of naturally occurring and synthetic compounds belonging to the flavonoid family. Structurally, chalcones consist of two aromatic rings connected through an α,β-unsaturated carbonyl system, which provides a highly conjugated framework capable of interacting with various biological targets.[1] Owing to their structural simplicity, synthetic accessibility, and versatile reactivity, chalcone derivatives have gained considerable interest in medicinal chemistry.[2] Numerous investigations have demonstrated that chalcones possess a wide spectrum of pharmacological properties, including antimicrobial, antioxidant, anti-inflammatory, anticancer, antimalarial, and enzyme inhibitory activities.[3–7] These biological properties make chalcones valuable scaffolds for the development of new therapeutic agents.[8]

Chemical modification of the chalcone backbone has been widely explored to enhance biological activity and improve pharmacological profiles.[9] Among the various structural modifications, the incorporation of sulfonate ester groups into chalcone frameworks has emerged as an attractive strategy for designing biologically active molecules.[10,11] Chalcone–sulfonate esters (Fig. 1) are hybrid structures in which the chalcone core is functionalized with sulfonate moieties (–SO_3R), providing additional electronic and steric characteristics that may influence biological interactions.[12] The presence of the sulfonate ester group can significantly alter physicochemical properties such as polarity, lipophilicity, and hydrogen-bonding capability, which may enhance the binding affinity of these molecules toward biological targets.[13]

[a]*Department of Chemistry, Govt. College Women University, Sialkot, 51300, Pakistan. E-mail: amina.sadiq@gcwus.edu.pk*

[b]*Department of Chemistry, University of Gujrat, Gujrat, 50700, Pakistan. E-mail: ehsan.ullah@uog.edu.pk*

[c]*Department of Pharmacognosy, Dow College of Pharmacy, Dow University of Health Sciences, Karachi, 74200, Pakistan*

[d]*Department of Chemical Engineering and Biotechnology, University of Cambridge, Cambridge, UK*

[e]*Department of Chemistry, Faculty of Science, King Khalid University, Abha, Saudi Arabia*

[f]*Chemistry Department, College of Science, Imam Mohammad Ibn Saud Islamic University (IMSIU) Riyadh, Saudi Arabia*

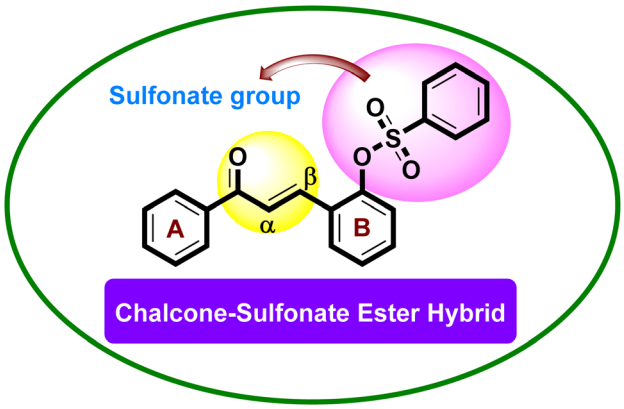

Fig. 1 Chemical structure of chalcone–sulfonate ester hybrid.

Sulfonate esters are well known in medicinal chemistry due to their role as useful pharmacophores in various bioactive compounds.[14] The strong electron-withdrawing nature of the sulfonyl group can modulate the electronic distribution within the chalcone scaffold, potentially increasing its electrophilicity and reactivity toward enzyme active sites.[15–17] Moreover, the sulfonate functionality can participate in additional intermolecular interactions such as hydrogen bonding, dipole–dipole interactions, and electrostatic contacts with amino acid residues in enzyme binding pockets.[18] As a result, chalcone–sulfonate esters have attracted increasing attention as promising candidates for the development of enzyme inhibitors and other biologically active molecules.[19,20]

Recent literature demonstrates the growing interest in chalcone–sulfonate derivatives as biologically active compounds.[21] For example, a series of chalcone derivatives containing thiophene–sulfonate groups were synthesized and evaluated for biological activity, and several compounds exhibited significant antibacterial and antiviral activities, suggesting that the incorporation of sulfonate groups can enhance biological potency.[22] Structural modification of chalcones with sulfonate esters and heterocyclic moieties such as thiophene has been shown to enhance their pharmacological potential. Recent studies reported that chalcone–sulfonate derivatives bearing thiophene exhibited strong enzyme inhibition, including pancreatic lipase and α-amylase, with IC_{50} values comparable to standard drugs, while molecular docking confirmed favorable binding interactions with enzyme active sites.[12,13]

Among the important enzymatic targets for therapeutic intervention, urease and α-amylase have been extensively studied due to their involvement in several pathological conditions. Urease is a nickel-dependent metalloenzyme that catalyzes the hydrolysis of urea into ammonia and carbon dioxide.[23] This reaction plays a crucial role in the survival and pathogenicity of ureolytic microorganisms, particularly *Helicobacter pylori*, which is responsible for gastritis, peptic ulcer disease, and gastric carcinoma.[24] Excessive urease activity is also associated with various medical complications, such as urinary tract infections, urolithiasis, and hepatic encephalopathy.[25]

Similarly, α-amylase is a key digestive enzyme responsible for the hydrolysis of dietary starch into oligosaccharides and glucose.[26,27] Inhibition of α-amylase is recognized as an effective approach for managing postprandial hyperglycemia in patients with type 2 diabetes mellitus.[28] By slowing down carbohydrate digestion and glucose absorption, α-amylase inhibitors help regulate blood glucose levels.[29]

In recent years, computational approaches have become valuable tools in modern drug discovery for understanding ligand–protein interactions and predicting the binding behaviour of small molecules with biological targets.[30] These studies complement experimental biological assays and provide insights into structure–activity relationships, facilitating the rational design of more potent compounds. In addition, DFT calculations are widely employed to investigate the electronic properties, molecular stability, and frontier molecular orbitals (HOMO–LUMO) of synthesized compounds, which are important for understanding their chemical reactivity and potential biological activity.[31,32] Furthermore, *in silico* ADME (absorption, distribution, metabolism, and excretion) analysis plays a crucial role in evaluating the pharmacokinetic properties and drug-likeness of candidate molecules, helping to predict their suitability as potential drug candidates in the early stages of drug discovery.[33]

In the present study, a series of chalcone–sulfonate ester derivatives was synthesized and characterized. The synthesized compounds, for the first time, were evaluated for their urease and α-amylase inhibitory activities using *in vitro* enzymatic assays. Furthermore, molecular docking studies were performed to explore the binding interactions of these compounds within the active sites of urease and α-amylase enzymes. DFT calculations and ADME predictions were also carried out to gain deeper insight into the electronic characteristics and pharmacokinetic properties of the synthesized molecules. This combined synthetic, biological, and computational investigation aims to explore the potential of chalcone–sulfonate esters as promising enzyme inhibitors and to provide insights for the development of new therapeutically relevant molecules.

2. Materials and methods

All chemicals and solvents were purchased from Sigma-Aldrich and were used without any purification. The NMR data were obtained in a Bruker Advance III 400 MHz spectrometer with a 5 mm BBI H-BB-D probe, 25 °C (293 K), in $CDCl_3$ solution. The chemical shifts (δ) are also given in parts per million (ppm) and the coupling constants (J) in hertz (Hz). The FTIR spectra were measured using a ThermoFisher Scientific FTIR spectrophotometer, and spectral positions were described in wavenumbers (cm^{-1}).

2.1. General procedure for the synthesis of chalcone–sulfonate esters

In step-1, 2-hydroxybenzaldehyde (1 mmol, 122 mg) was dissolved in ethanol (10 mL) in a round-bottom flask equipped with a magnetic stirrer. An 8% aqueous solution of sodium hydroxide (1 mmol, 0.04 mL) was then added dropwise to the reaction mixture under continuous stirring. The mixture was

stirred for 30 minutes to ensure proper mixing and activation of the aldehyde component. Subsequently, acetophenone (1 mmol, 120 mg) was added dropwise to the reaction mixture. The resulting reaction mixture was allowed to stir at room temperature for 24 hours. The progress of the reaction was monitored by thin-layer chromatography (TLC). After completion, the reaction mixture was carefully neutralized using dilute hydrochloric acid until the pH reached approximately 7, which led to the formation of a yellow precipitate. The precipitated solid was collected by filtration, thoroughly washed with distilled water, and allowed to dry. The crude product was purified by recrystallization from methanol (5–10 mL) to obtain pure yellow crystalline 2-hydroxychalcone. The crystals were further rinsed with chilled methanol to remove any remaining impurities.[12]

In step-2, 2-hydroxychalcone (1 mmol, 146 mg) and triethylamine (TEA) (1.2 mmol, 0.17 mL) were dissolved in dimethylformamide (DMF, 10 mL) in a conical flask. The reaction mixture was cooled in an ice bath and stirred for 30 minutes to stabilize the reaction environment. Following this, the appropriate aryl benzenesulfonyl chloride (1 mmol, 190–220 mg, depending on the nature of the aryl substituent) was added dropwise to the chilled reaction mixture. The reaction was then allowed to proceed under continuous stirring at room temperature for 24 hours. Upon completion of the reaction, the mixture was poured into ice-cold water (50 mL), which induced the precipitation of the desired product. The resulting solid was collected by filtration, thoroughly washed with distilled water, and dried. The crude precipitate was purified by recrystallization from methanol (5–10 mL). The obtained crystals were further washed with chilled methanol to remove any residual impurities, yielding the chalcone–sulfonate ester derivatives in high purity.[12,14]

2.1.1. Spectroscopic data of synthesized compounds

*2.1.1.1 (E)-2-(3-Oxo-3-phenylprop-1-en-1-yl)phenyl 2,4,6-trimethylbenzenesulfonate (**1**).*

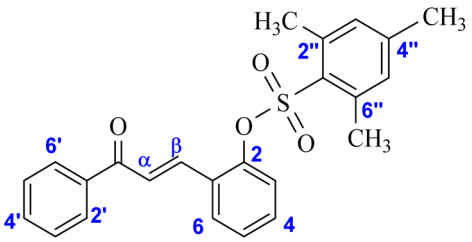

Bright yellow powder, yield: 87%; MP 108–110 °C; FTIR (cm^{-1}): 3082, 1696, 1564, 1469, 1372, 1222, 1191, 769; ^{1}H NMR (400 MHz, $CDCl_3$) δ 7.97–7.92 (m, 4H, Ar–H), 7.66–7.63 (m, 2H, Ar–H), 7.61–7.54 (m, 1H, Ar–H), 7.52–7.49 (m, 2H, Ar–H), 7.22–7.19 (m, 2H, Ar–H), 6.85 (s, 2H, Ar–H), 2.48 (s, 6H, 2 × CH_3), 2.10 (s, 3H, CH_3); ^{13}C NMR (101 MHz, $CDCl_3$) δ 190.0, 148.3, 144.0, 140.5, 138.0, 137.7, 136.4, 133.5, 132.8, 132.0, 131.1, 130.4, 129.3, 128.6, 128.2, 128.0, 127.2, 124.3, 124.1, 23.0, 20.8; accurate mass (ESI) of $[M + H]^+$: calculated for $C_{24}H_{23}O_4S$ 407.1307; found 407.1312.

*2.1.1.2 2-[(1E)-3-Oxo-3-phenylprop-1-en-1-yl]phenyl 4-bromobenzene-1-sulfonate (**2**).*

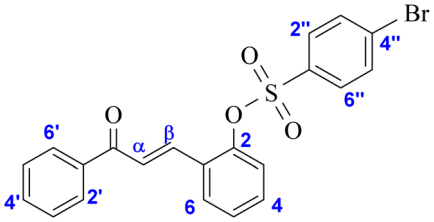

Pale yellow powder, yield: 87%; MP 122–124 °C; FTIR (cm^{-1}): 3067, 1654, 1570, 1442, 1376, 1266, 1195, 791; ^{1}H NMR (400 MHz, $CDCl_3$) δ 7.98–7.91 (m, 2H, Ar–H), 7.67–7.56 (m, 4H, Ar–H), 7.57 (d, J = 15.8 Hz, 1H, H-β), 7.56–7.48 (m, 4H, Ar–H), 7.48–7.41 (m, 1H, Ar–H), 7.40–7.30 (m, 2H, Ar–H), 7.26 (d, J = 15.8 Hz, 1H, H-α); ^{13}C NMR (101 MHz, $CDCl_3$) δ 189.7 (C=O), 148.1, 137.7, 137.2, 133.8, 133.0, 132.7, 131.5, 130.0, 129.9, 128.8, 128.7, 128.6, 128.0, 127.7, 124.4 and 124.0; accurate mass (ESI) of $[M + H]^+$: calculated for $C_{21}H_{16}BrO_4SNa$ 442.9952; found 442.9946.

*2.1.1.3 2-[(1E)-3-Oxo-3-phenylprop-1-en-1-yl]phenyl 4-methoxybenzene-1-sulfonate (**3**).*

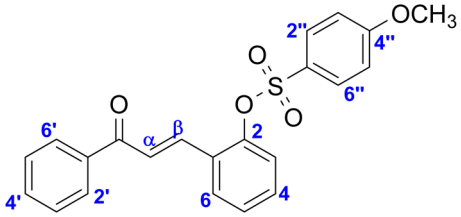

Bright yellow powder, yield: 78%; MP 104–106 °C; FTIR (cm^{-1}): 3054, 1660, 1571, 1451, 1355, 1180, 1012, 792; ^{1}H NMR (600 MHz, $CDCl_3$) δ 7.92 (br d, J = 8.6 Hz, 2H, Ar–H), 7.65 (d, J = 8.9 Hz, 2H, Ar–H), 7.62–7.57 (m, 2H, Ar–H), 7.56 (d, J = 15.8 Hz, 1H, H-β), 7.50 (br td, J = 7.6, 1.4 Hz, 2H, Ar–H), 7.44–7.40 (m, 1H, Ar–H), 7.38 (br d, J = 7.6 Hz, 1H, Ar–H), 7.31 (td, J = 7.5, 1.4 Hz, 1H, Ar–H), 7.21 (d, J = 15.8 Hz, 1H, H-α), 6.80 (d, J = 8.9 Hz, 2H, Ar–H), 3.59 (s, 3H, OCH_3); ^{13}C NMR (151 MHz, $CDCl_3$) δ 189.9, 164.4, 148.4, 137.8, 137.7, 133.1, 131.5, 130.9, 129.1, 128.8, 128.7, 128.6, 127.9, 127.5, 124.4, 124.0, 114.6, 55.5; accurate mass (ESI, –ve) of $[M]^-$: calculated for $C_{22}H_{18}O_5S$ 394.0880; found 394.0757.

*2.1.1.4 2-[(1E)-3-Oxo-3-phenylprop-1-en-1-yl]phenyl 4-chlorobenzene-1-sulfonate (**4**).*

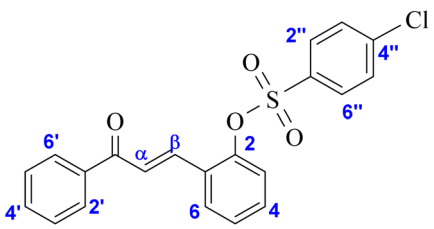

Bright yellow powder, yield: 56%; MP 128–130 °C; FTIR (cm^{-1}): 3065, 1652, 1576, 1474, 1389, 1279, 1152, 774; ^{1}H NMR (400

MHz, $CDCl_3$) δ 7.97–7.90 (m, 2H, Ar–H), 7.71 (d, J = 8.7 Hz, 2H, Ar–H), 7.64 (dd, J = 7.8, 1.7 Hz, 1H, Ar–H), 7.64–7.57 (m, 1H, Ar–H), 7.58 (d, J = 15.8 Hz, 1H, H-β), 7.51 (t, J = 7.5 Hz, 2H, Ar–H), 7.45 (ddd, J = 8.7, 7.2, 1.7 Hz, 1H, Ar–H), 7.40–7.31 (m, 4H, Ar–H), 7.27 (d, J = 15.8 Hz, 1H, H-α); ^{13}C NMR (101 MHz, $CDCl_3$) δ 189.8 (C=O), 148.1, 141.4, 137.7, 137.2, 133.3, 133.0, 131.5, 129.9, 129.7, 128.8, 128.7, 128.5, 128.0, 127.7, 124.4 and 124.0; accurate mass (ESI) of $[M + Na]^+$: calculated for $C_{21}H_{15}ClO_4SNa$ 421.0277; found 421.0270.

*2.1.1.5 2-[(1E)-3-Oxo-3-phenylprop-1-en-1-yl]phenyl naphthalene-2-sulfonate (**5**).*

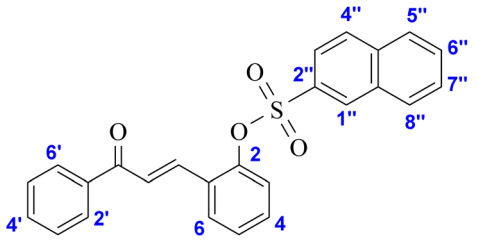

Pale yellow powder, yield: 83%; MP 112–114 °C; FTIR (cm^{-1}): 3057, 1658, 1573, 1481, 1377, 1280, 1154, 785; ^{1}H NMR (400 MHz, $CDCl_3$) δ 7.97–7.93 (m, 1H, Ar–H), 7.84 (d, J = 8.3 Hz, 2H, Ar–H), 7.76 (dd, J = 8.7, 1.9 Hz, 1H, Ar–H), 7.74–7.67 (m, 3H, Ar–H), 7.60 (d, J = 15.8 Hz, 1H, H-β), 7.57–7.52 (m, 2H, Ar–H), 7.52–7.46 (m, 2H, Ar–H), 7.46–7.38 (m, 4H, Ar–H), 7.35–7.28 (m, 1H, Ar–H), 7.06 (d, J = 15.8 Hz, 1H, H-α); ^{13}C NMR (101 MHz, $CDCl_3$) δ 189.5, 148.3, 137.5, 137.5, 135.4, 133.5, 132.8, 131.9, 131.8, 131.5, 130.6, 129.6, 129.6, 129.4, 129.0, 128.6, 128.5, 128.4, 128.2, 128.1, 127.9, 127.7, 127.5, 124.12, 124.07, 122.9; accurate mass (ESI) of $[M + Na]^+$: calculated for $C_{25}H_{18}O_4SNa$ 437.0824; found 438.0843.

*2.1.1.6 2-[(1E)-3-Oxo-3-phenylprop-1-en-1-yl]phenyl 2-chlorobenzene-1-sulfonate (**6**).*

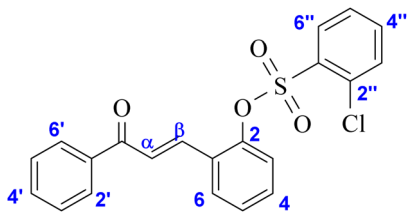

Pale yellow powder, yield: 81%; MP 79–81 °C; FTIR (cm^{-1}): 3055, 1665, 1565, 1447, 1394, 1280, 1161, 765; ^{1}H NMR (400 MHz, $CDCl_3$) δ 7.96–7.91 (m, 3H, Ar–H), 7.82 (d, J = 15.9 Hz, 1H, H-β), 7.68 (dd, J = 7.6, 1.9 Hz, 1H, Ar–H), 7.63–7.54 (m, 1H, Ar–H), 7.55–7.43 (m, 4H, Ar–H), 7.39 (ddd, J = 8.0, 7.4, 1.9 Hz, 1H, Ar–H), 7.34–7.30 (m, 2H, Ar–H), 7.33 (d, J = 15.9 Hz, 1H, H-α), 7.28 (dd, J = 7.4, 1.8 Hz, 1H, Ar–H); ^{13}C NMR (101 MHz, $CDCl_3$) δ 190.3, 148.1, 137.8, 137.8, 135.3, 133.8, 133.7, 133.5, 132.9, 132.5, 132.0, 131.3, 129.1, 128.7, 128.3, 128.2, 127.6, 127.1, 125.1, 123.8; accurate mass (ESI) of $[M + Na]^+$: calculated for $C_{21}H_{15}ClO_4SNa$ 421.0277; found 421.0265.

*2.1.1.7 (E)-2-(3-Oxo-3-phenylprop-1-en-1-yl)phenyl 2-nitrobenzenesulfonate (**7**).*

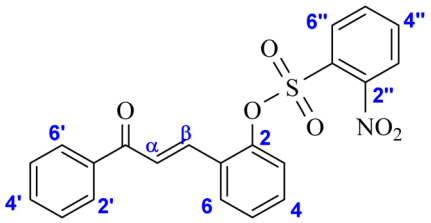

Pale yellow powder, yield: 87%; MP 135–137 °C; FTIR (cm^{-1}): 3092, 1736, 1607, 1444, 1384, 1253, 1143, 774; ^{1}H NMR (400 MHz, $CDCl_3$) δ 7.96–7.92 (m, 4H, Ar–H), 7.69 (dd, J = 8.0, 4.0, Hz, 1H, Ar–H), 7.61–7.57 (m, 1H, Ar–H), 7.52–7.46 (m, 4H, Ar–H), 7.39 (dd, J = 8.0, 4.0, Hz, 1H, Ar–H), 7.36–7.26 (m, 4H, Ar–H); ^{13}C NMR (101 MHz, $CDCl_3$) δ 190.2, 148.1, 137.8, 137.7, 135.2, 133.7, 133.5, 132.8, 132.0, 131.30, 129.0, 128.6, 128.2, 127.6, 127.1, 125.1, 123.7; accurate mass (ESI) of $[M + H]^+$: calculated for $C_{21}H_{16}NO_6S$ 410.0698; found 410.0689.

2.2. Determination of urease and α-amylase inhibitory activities

2.2.1. Urease and α-amylase inhibitory activities. The experimental protocols for the α-amylase and urease assays were carried out following previously reported literature methods.[25,34]

2.3. *In silico* investigations

2.3.1. SwissADME. The SwissADME online server was used to evaluate the pharmacokinetic properties of the synthesized chalcone sulfonate esters based on SMILES notation. The study assessed key ADME parameters, including drug-likeness, GI absorption, and BBB permeability.[35] A detailed computational workflow is provided in the SI.

2.3.2. Molecular docking

2.3.2.1 Protein selection and protein preparation. Molecular docking studies were performed to investigate the binding interactions of the synthesized compounds with urease and α-amylase enzymes using Molegro Virtual Docker. Protein targets and ligands were prepared prior to docking, and binding affinities were evaluated using standard docking protocols. Crystal structures of urease (1OTH, 2ZAV) and α-amylase (1SMD, 5U3A) were obtained from the Protein Data Bank (Table S1). Proteins were prepared for docking by removing water molecules and optimizing active sites.[36] Full methodological details are provided in the SI file.

2.3.2.2 Ligand preparation. The synthesized compounds and reference drugs were energy-minimized and converted into appropriate formats for docking studies.[37] Ligand optimization and preparation steps are described in detail in the SI file.

2.3.2.3 Molecular docking assay. Docking simulations were performed using MVD to predict binding modes and affinities of ligands within enzyme active sites. The best poses were selected based on MolDock scores.[38,39] Full docking protocol details are provided in the SI file.

2.3.2.4 Visualization. Protein–ligand interactions were analyzed using 2D and 3D visualization tools to identify

hydrogen bonding and hydrophobic interactions.[40] Details of visualization software and parameters are provided in the SI file.

2.3.2.5 Validation of docking. Docking accuracy was validated using redocking of co-crystallized ligands, and RMSD values were used to assess reliability.[41] A full validation protocol is provided in the SI file.

2.4. MD simulation

Molecular dynamics simulations were performed to evaluate the stability of selected protein–ligand complexes using WebGRO (GROMACS). Structural stability was analysed over 25 ns simulation time.[42,43] Detailed simulation parameters are provided in the SI file.

2.5. Density functional theory (DFT)

DFT calculations were performed using Gaussian 09 at the B3LYP/6-311G level to investigate electronic properties of selected compounds. Frontier molecular orbitals and reactivity descriptors were analyzed.[44–47] Complete computational details are provided in the SI file.

3. Results and discussion

3.1. Chemistry

A series of chalcone-hybrid compounds was synthesized *via* Claisen–Schmidt condensation using simple acetophenone and salicylaldehyde as starting materials. The intermediate 2-hydroxychalcone subsequently reacted with various aryl sulfonyl chlorides to afford the target chalcone–sulfonate derivatives. Using a triethylamine (TEA) base/substrate ratio of 1 : 1, five novel substituted chalcone–sulfonate compounds (**1–7**) were obtained after stirring for 65 min under ice-cold conditions (0–5 °C) (Scheme 1).

The synthesized chalcone sulfonate ester was characterized using FT-IR, NMR, and mass spectrometry techniques. In the FT-IR spectrum, the absorption band at 3065 cm^{-1} corresponds to aromatic C–H stretching, while the strong band at 1652 cm^{-1} is attributed to the conjugated carbonyl (C=O) group of the chalcone moiety. Additional bands at 1576, 1474, and 1389 cm^{-1} indicate aromatic C=C vibrations, whereas the peaks at 1279 and 1152 cm^{-1} confirm the presence of the sulfonate (S=O) functional group; the band at 774 cm^{-1} is assigned to aromatic C–H out-of-plane bending. The ^{1}H NMR spectrum shows multiple signals in the aromatic region (δ 7.97–7.31 ppm) corresponding to protons of substituted phenyl rings. The characteristic *trans*-olefinic protons of the chalcone framework appear as doublets at δ 7.58 and 7.27 ppm with a large coupling constant (J = 15.8 Hz), confirming the *E*-configuration of the α,β-unsaturated system. The ^{13}C NMR spectrum further supports the structure by displaying a carbonyl carbon resonance at δ 189.8 ppm along with several signals between δ 148.1–124.0 ppm corresponding to aromatic and olefinic carbons. High-resolution mass spectrometry also corroborated the structural assignment obtained from the spectroscopic techniques.

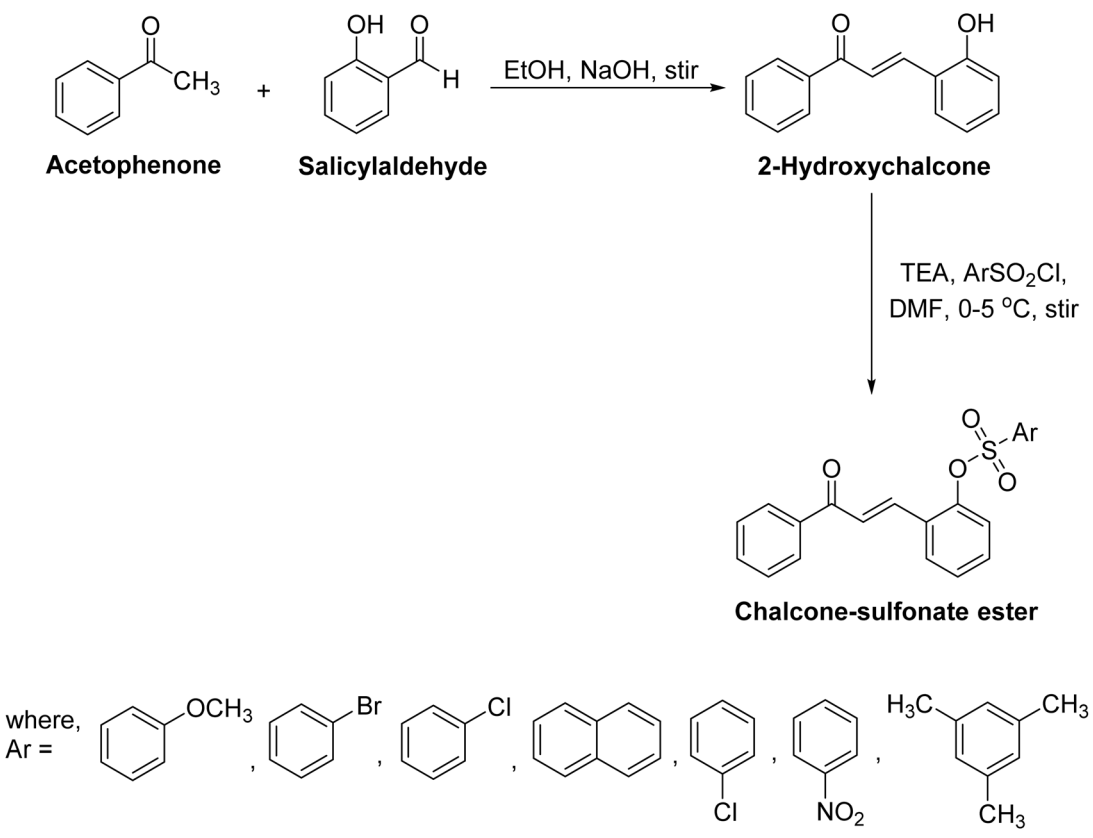

Scheme 1 Synthesis of chalcone-sulfonate esters/hybrid compounds (**1–7**).

3.2. Urease and α-amylase inhibitory activities

The synthesized series of chalcone–sulfonate derivatives (**1–7**) was evaluated for their inhibitory potential against urease and α-amylase enzymes (Table 1). The inhibitory activity was expressed as IC_{50} values (μM) and compared with standard inhibitors, thiourea for urease and acarbose for α-amylase. Overall, the compounds demonstrated moderate to excellent enzyme inhibition, suggesting that substitution on the benzenesulfonate moiety significantly influences biological activity.

For urease inhibition, IC_{50} values ranged from 6.5 to 19.5 μM, whereas for α-amylase inhibition, the values varied between 5.2 and 27.5 μM. Several derivatives displayed stronger inhibitory activity than the standard drug in at least one assay, highlighting the therapeutic potential of this structural scaffold. Compound **7**, containing 2-nitrobenzenesulfonate substituent, showed high inhibition of urease activity (IC_{50} = 6.5 ± 0.3 μM), which was found to be significantly more potent than the standard thiourea (21.0 ± 0.9 μM). Similarly, compound **5** with a naphthalene-2-sulfonate moiety was found to be the most potent among the tested derivatives with an IC_{50} value of 6.9 ± 0.3 μM and 5.2 ± 0.6 μM against urease and α-amylase, respectively. In comparison, compound **3**, with a 4-methoxybenzenesulfonate group, was comparatively less active with IC_{50} values of 19.5 ± 1.0 μM and 20.6 ± 0.9 μM against urease and the α-amylase, respectively.

3.2.1. Structure–activity relationship (SAR) analysis. SAR reveals clearly that electronic and steric properties of the substituents on the sulfonate aromatic ring are decisive determinants of enzyme inhibitory activity.

First, the presence of electron-withdrawing substituents significantly enhanced enzyme inhibition. Compound **7** showed strong urease and α-amylase inhibitory activities because it contains a nitro group at the *ortho* position. The nitro group strongly attracts electrons, which results in increased electrophilic properties for the chalcone system to create greater binding strength with active site residues of the enzyme.

The halogenated derivatives showed better inhibitory effects than their unsubstituted or electron-donating counterparts. Compound **2** with a *p*-bromo substituent showed strong α-amylase inhibition which had an IC_{50} value of 9.8 ± 0.7 μM because the larger halogen atom improves hydrophobic binding interactions inside the enzyme binding pocket. Compound **4**, which contains a *p*-chloro group, showed moderate enzyme activity because halogen substitution produces hydrophobic and electronic effects that improve enzyme function.

Compound **5** showed the strongest dual inhibition effect because it contains a bulky naphthalene-2-sulfonate moiety, which most effectively inhibits the tested molecules. The naphthalene ring extended aromatic system creates additional π–π stacking interactions, which establish hydrophobic contacts with the enzyme active site to stabilize the enzyme–inhibitor complex and increase inhibitory strength.

In contrast, derivatives bearing electron-donating groups tended to show reduced activity. The methoxy substituent in compound **3** showed decreased inhibition effects against both studied enzymes. The presence of electron-donating substituents causes a decline in electrophilicity for the chalcone carbonyl system, which leads to decreased beneficial interactions with catalytic residues. The activity of compound **1**, which contains trimethyl substituents, remained at a low level because its steric hindrance and decreased electron-withdrawing power restricted its effectiveness. The positioning of substituents on a compound proves to have important effects. The compound **7**, which contains an *o*-chloro group, demonstrated moderate inhibitory effects, which were less than those shown by the *p*-substituted analogue compound **4**, because the sulfonate linkage area created steric hindrance that limited enzyme binding efficiency.

Among the synthesized compounds, compound **5** and compound **7** emerged as the most promising dual inhibitors, displaying stronger activity than the reference drugs in at least one assay. These findings suggest that structural optimization focusing on strong electron-withdrawing substituents and extended aromatic frameworks could further improve the potency of this class of compounds.

Table 1 Inhibition of urease and α-amylase activities by the synthesized compounds (**1–7**)

	Urease	α-Amylase
Compound no.	IC_{50} ± SEM (μM)	IC_{50} ± SEM (μM)
1	16.8 ± 0.9	27.5 ± 1.2
2	10.2 ± 0.5	9.8 ± 0.7
3	19.5 ± 1.0	20.6 ± 0.9
4	9.4 ± 0.4	17.9 ± 0.8
5	6.9 ± 0.3	5.2 ± 0.6
6	12.6 ± 0.6	13.6 ± 0.7
7	6.5 ± 0.3	7.8 ± 0.5
Standard	21.0 ± 0.9 (Thiourea)[a]	12.0 ± 0.5 (Acarbose)[a]

[a] Used as a positive control for urease and α-amylase enzymes.

3.3. SwissADME analysis

SwissADME online server was used to determine the pharmacokinetic and drug-like properties of the synthesized chalcone sulfonate ester derivatives (**1–7**). The resulting values of the physicochemical descriptors, lipophilicity, water solubility, pharmacokinetics, and medicinal chemistry characteristics are summarized in Table S2 in the SI file, and the general drug-likeness profile and absorption forecasts are shown in Fig. 2 (bioavailability radar) and Fig. 3 (BOILED-Egg model).

3.3.1. Physicochemical properties. Physicochemical properties of all the synthesized compounds were analyzed to identify their appropriateness as a potential drug candidate. According to Table S2 in the SI file, the molecular weight (MW) of the compounds was between 394.44 and 443.31 g mol^{-1}, which is within the acceptable range of orally active drugs (less than 500 g mol^{-1}). Compounds **3** (394.44 g mol^{-1}) and **4** (398.86 g mol^{-1}) had relatively low molecular weights, which indicates good permeability of the membrane and oral bioavailability.

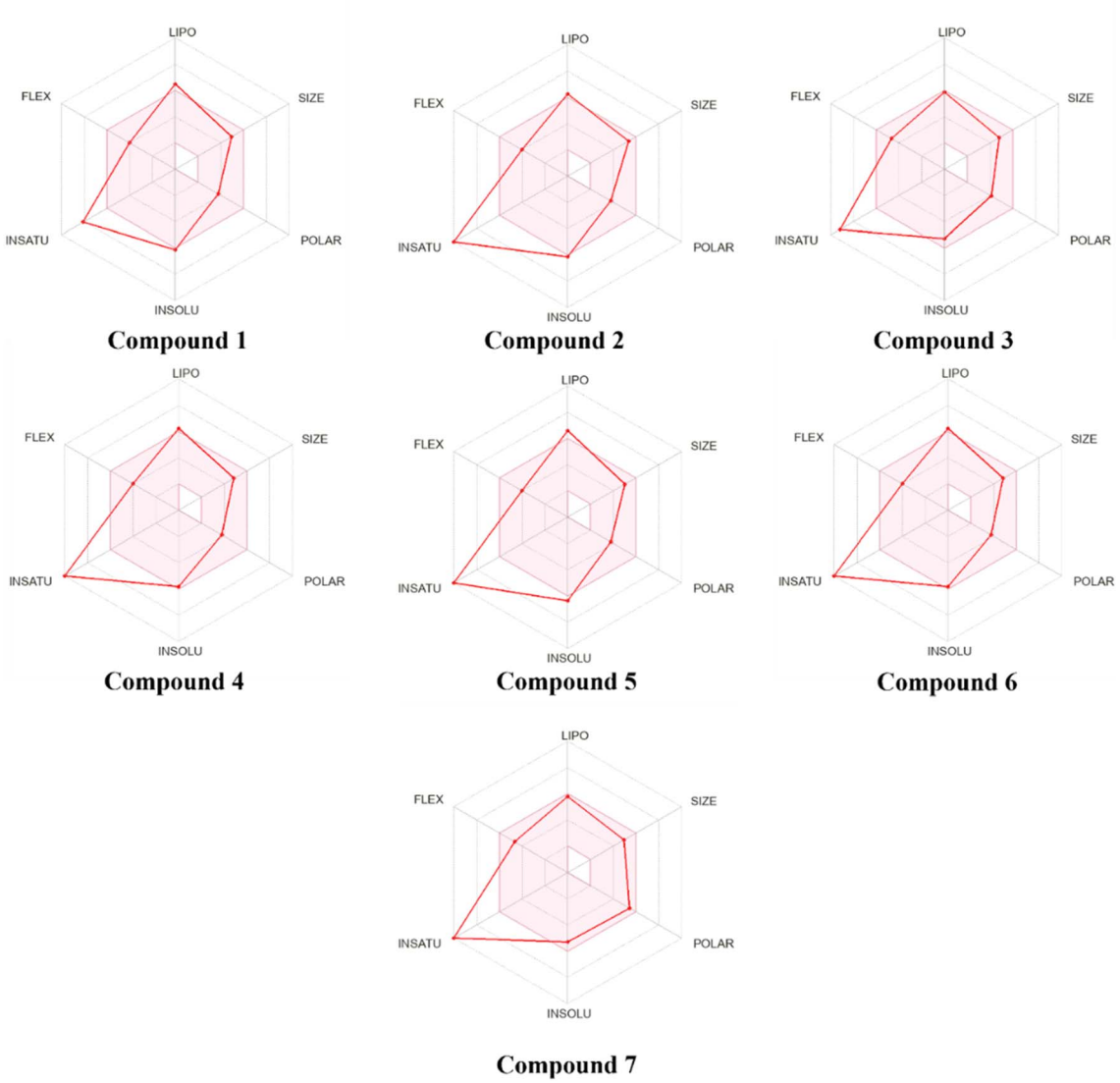

Fig. 2 ADME radar of synthesized compounds (**1–7**).

Hydrogen bond acceptors were 4 to 6, and hydrogen bond donors were 0 to 1, which met the requirements of the recommendation of drug-like molecules. Topographical polar surface area (TPSA) observed a range of 68.82 to 114.64 Å, which falls within the acceptable range (less than 140 Å) of intestinal absorption. It is important to note that compounds (**1–7**) had TPSA values of 68.82 Å, which demonstrated great potential of passive diffusion through the membrane. Compound 7 (114.64 Å) had a relatively higher polarity, however, which could decrease the permeability of the membrane. According to these descriptors, compounds **3**, **4**, and **6** may be regarded as one of the most appropriate variants as they have a balanced molecular size and polarity.

3.3.2. Lipophilicity. Lipophilicity is a major parameter that affects the membrane permeability and the distribution of drugs. Table S2 in the SI file displays the results of the predicted lipophilicity values of various algorithms (iLOGP, XLOGP3, WLOGP, MLOGP, and Silicos-IT) and the overall trend line is given by the consensus log *P* values. The values of consensus log *P* that were within the range of 3.47 to 5.21 meant moderate to high lipophilicity. Compound **1** ($\log P = 5.21$) exhibited a comparatively greater lipophilicity, which could positively impact membrane permeability but may have a negative effect on solubility. Conversely, compound 7 ($\log P = 3.47$) had more balanced lipophilicity values in the ranges of drug friendliness (**1–4**). Thus, compounds 7 and **3** could be discussed as the most reasonable options regarding the balanced lipophilicity and drug-like properties.

3.3.3. Water solubility. The solubility of water is also important in drug absorption and bioavailability. Table S2 in the SI file shows the predicted values of ESOL log *S* and solubility classes. The majority of the compounds were characterized as poorly soluble with a range of −6.41 to −6.13. Compounds **3**, **4**, **6**, and **7** were, however, predicted to be moderately soluble, which is favorable in oral drug formulations. Compounds 7 ($\log S = -5.29$) and **3** showed the best

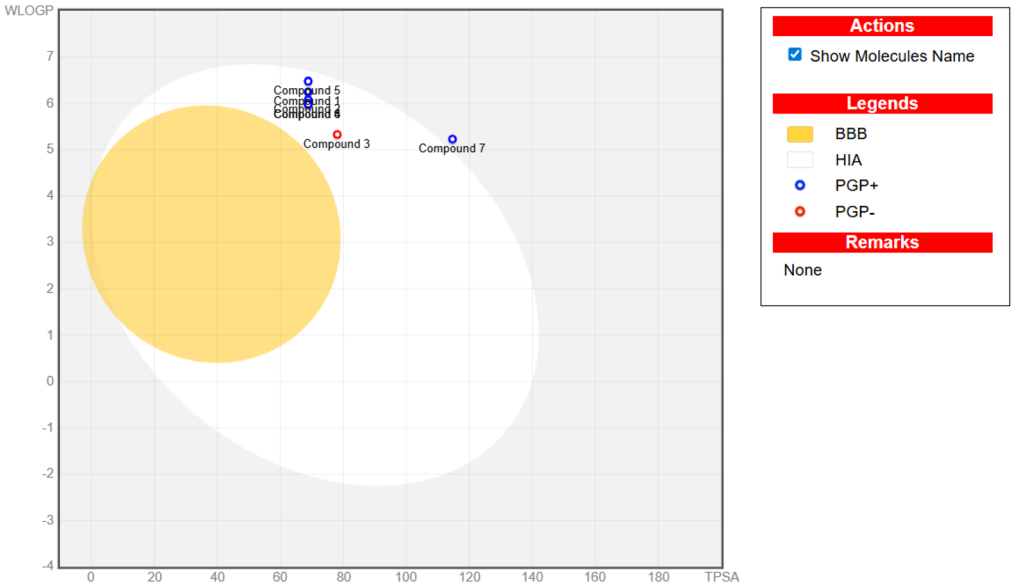

Fig. 3 BOILED-egg of ADME study synthesized compounds (**1–7**).

predicted solubility. These compounds thus may have better dissolution characteristics as well as increased gastrointestinal absorption than the other derivatives.

3.3.4. Pharmacokinetic properties. Table S2 in the SI file summarizes the predicted pharmacokinetic profile using SwissADME, whereas the absorption properties are presented through the BOILED-Egg model (Fig. 3). The majority of the compounds (**1–6**) were expected to show high gastrointestinal (GI) absorption and hence good oral bioavailability. Compound **7**, on the other hand, recorded low GI absorption, which is probably because of its increased polarity and TPSA. No compounds were predicted to be blood–brain barrier (BBB) permeant, and this implies that these compounds might be less likely to penetrate the central nervous system, which may be advantageous in limiting the neurological side effects. In terms of interactions with efflux transporters, the majority of the compounds were predicted to have interaction with the P-glycoprotein, with the exception of compound **3**, are likely to have better retention in the cell. Moreover, some compounds were found to exhibit inhibitory activity against some cytochrome P450 enzymes, especially CYP2C19 and CYP2C9, but none were predicted to inhibit CYP2D6 or CYP3A4, indicating that there has been a low risk of drug–drug interaction with metabolism. Based on the overall pharmacokinetic profile, compound **3** was the most promising candidate as they have high GI absorption and neither has a P-glycoprotein substrate feature.

3.3.5. Drug-likeness evaluation. The analysis of drug-likeness was done based on various established filters such as Lipinski, Ghose, Veber, Egan, and Muegge filters. The findings summarized in Table S2 in the SI file show that the majority of compounds did not violate the Lipinski rule more than once, also, in most cases, because of high lipophilicity. Compounds **3** and **7**, however, indicated zero Lipinski violations, indicating high adherence to drug-likeness criteria. In addition, the Veber rule was met by all compounds, which meant that oral bioavailability was reasonable regarding molecular flexibility and polar surface area. It is expected that the bioavailability score of all compounds (0.55) was not high, as is normally the case with compounds that are well absorbed orally. According to these requirements, it can be said that compounds **3** and **7** are the most promising drug-like molecules of the series synthesized.

3.3.6. Medicinal chemistry assessment. Medicinal chemistry filters were also examined to determine possible structural alerts. All of the compounds indicated no traces of PAINS (Pan-Assay Interference Compounds) as observed in Table S2 in the SI file, which means that the molecules are unlikely to yield false-positive biological results. Nevertheless, most compounds were alerted to compound **7** with four alerts, which may indicate structural liabilities. The scores of synthetic accessibilities were between 3.40 and 3.84, which is a sign that the compounds have an average synthetic feasibility. Compound **4** (3.44) had relatively easier accessibility regarding synthesis.

Altogether, the SwissADME revealed the fact that most of the synthesized chalcone sulfonate ester derivatives have good pharmacokinetic and drug-likeness characteristics. Out of the examined molecules, **3** and **7** turned out to be the best possible options, since they do not violate Lipinski's rule, exhibit high GI absorption, moderate solubility, moderate lipophilicity, and decent medicinal chemistry behavior. The bioavailability radar (Fig. 2) also substantiates the pleasant physicochemical space of these compounds, and the predicted gastrointestinal absorption characteristics of these compounds are validated using the BOILED-Egg model (Fig. 3). These results imply that compounds **3** and **7** can be used as possible lead molecules to conduct further biological assessment and drug development activities.

3.4. Molecular docking analysis

Molecular docking simulations were performed to determine the affinity of binding and the mechanism of interaction

between the synthesized chalcone sulfonate ester derivatives and the target enzymes surrounding the urea metabolism and carbohydrate metabolism. Docking experiments also give structural information on the ligand–protein interactions by predicting a ligand with the most stable orientation with the active site of a protein. In the current research, synthesized compounds (**1–7**) were docked against two urease related proteins (1OTH and 2ZAV) and two α-amylase proteins (1SMD and 5U3A) by Molegro Virtual Docker. The synthesized derivatives were compared to the performance of the docking with the reference inhibitors thiourea (urease inhibitor) and acarbose (α-amylase inhibitor). The results of the computation of the MolDock scores, hydrogen bonding, and hydrophobic contacts are presented in Table S3 and S4 in SI file, whereas the plot of the chosen complexes between proteins and their ligands is depicted in Fig. 4–11. The docking score (MolDock score) is an expression of the predicted binding affinity of the ligand with the active site of the enzyme. A decrease in docking scores implies that there is greater binding interaction and increased binding stability. Besides docking scores, types of interaction like hydrogen bonding, π–π interactions, and hydrophobic contacts are significant in the stabilization of the ligand in the enzyme binding site.

3.4.1. Docking analysis *versus* urease proteins

3.4.1.1 The interaction with the 1OTH protein. The docking study *versus* the urease-related protein 1OTH revealed good binding affinities to a number of synthesized chalcone sulfonate derivatives. The interaction profiles and docking scores are shown in Table S3 in the SI file. Compound **7** was one of the studied compounds with the best docking score, indicating that it has a high binding affinity with the enzyme catalytic pocket. The interaction analysis showed that the ligand established numerous hydrogen bonding interactions with important residues that are related to the binding of the substrate. Like other active compounds, hydrogen bond interactions were predominantly found to the residues of ARG270, ASN198, HIS202, and SER267, which are found in the active region of the protein. The binding affinity is also increased by these hydrogen bonds, which stabilize the ligand in the binding cavity.

Besides hydrogen bonding, there were a number of hydrophobic interactions noted between the aromatic rings of the chalcone backbone and other hydrophobic residues within the protein, including ASP165, LEU166, and ARG270. Such interactions comprise π–alkyl and amide–π stacked interactions, which also lead to the stabilization of the protein complex with the ligand. Fig. 4 depicts the spatial orientation of compound **8** in the active pocket of the 1OTH protein, the three-dimensional complex, hydrophobic interactions and the two-dimensional interaction diagram.

By way of comparison, the interaction pattern of the same protein with the reference inhibitor, thiourea, is displayed in Fig. S1 in the SI file. Though thiourea has the capacity of making hydrogen bonds in the binding pocket, the interaction network

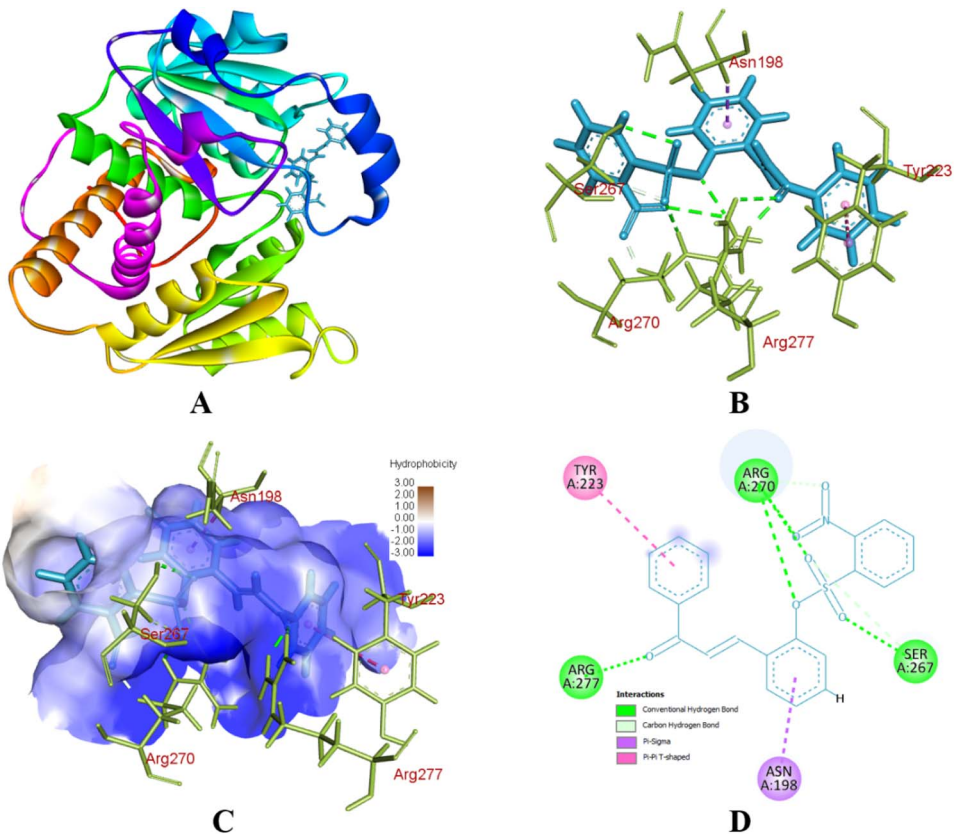

Fig. 4 Interaction of 1OTH protein with compound **7** (A) structure of protein (B) protein–ligand interaction (C) hydrophobic interaction (D) 2D diagram of ligand.

and the docking score of compound 7 reveals that it is more stabilized in the catalytic site. Hydrophobic interactions of the chalcone framework with the other residues are likely to be increased by the presence of aromatic rings and long conjugation in the structure, thus improving the binding affinity.

3.4.1.2 The interaction with 2ZAV protein. Additional docking was done against the second protein related to urease, 2ZAV, and the output is also given in Table S3 in the SI file. The compounds displayed good binding orientations in the active cavity of the enzyme. Compound 7 was once again found to have binding interactions with the 2ZAV protein as one of the tested derivatives. The ligand forms stabilizing hydrogen bonding interactions with active site residues and retains a good orientation in the catalytic pocket. According to the interaction diagram in Fig. 5, the active site is well accommodated with the compound and is hydrogen-bonded and hydrophobically interacting with the amino acid residues around the active site. The hydrophobic residues are π–alkyl intermolecular interactions with the aromatic rings of the chalcone structure, and thus, contribute to the stability of the complex between the protein and the ligand. These interactions are significant in keeping the ligand in the active cavity and enhancing the inhibitory potential. Fig. S2 in the SI file shows the docking action of the reference inhibitor thiourea with the 2ZAV protein. The interaction of thiourea with multiple active site residues is supported by hydrogen bonding, but the docking score and interaction network with compound 7 indicate that this compound has a higher binding affinity and improved stabilization in the enzyme active site. The general trend of docking outcomes with urease proteins shows that compound 7 has the most promising interaction profile, which consists of multiple hydrogen bonds and hydrophobic contacts with key catalytic residues. Such interactions affirm their possible usage as a lead compound as a urease inhibitor.

3.4.2. Docking analysis against α-amylase proteins

3.4.2.1 Interaction with 1SMD protein. Docking experiments were also done to determine the binding properties of the synthesized products with the salivary protein 1SMD. Table S4 in the SI file shows a summary of the docking scores and interaction details. Compound 5 exhibited the best docking profile with the 1SMD protein of all the derivatives studied. Despite the small amount of hydrogen bonding contacts that were noted, the ligand establishes a large network of hydrophobic interactions with residues present in the active site of the enzyme. The contact analysis showed contacts with the residues of TYR62, HIS201, TRP58, TRP59, HIS305, ALA198, LYS200, and ILE235. These are π–π stacked interactions, π–π T-shaped interactions, and π-alkyl interactions that play an important role in the stabilization of the ligand in the binding pocket. Another factor that influences the manner in which

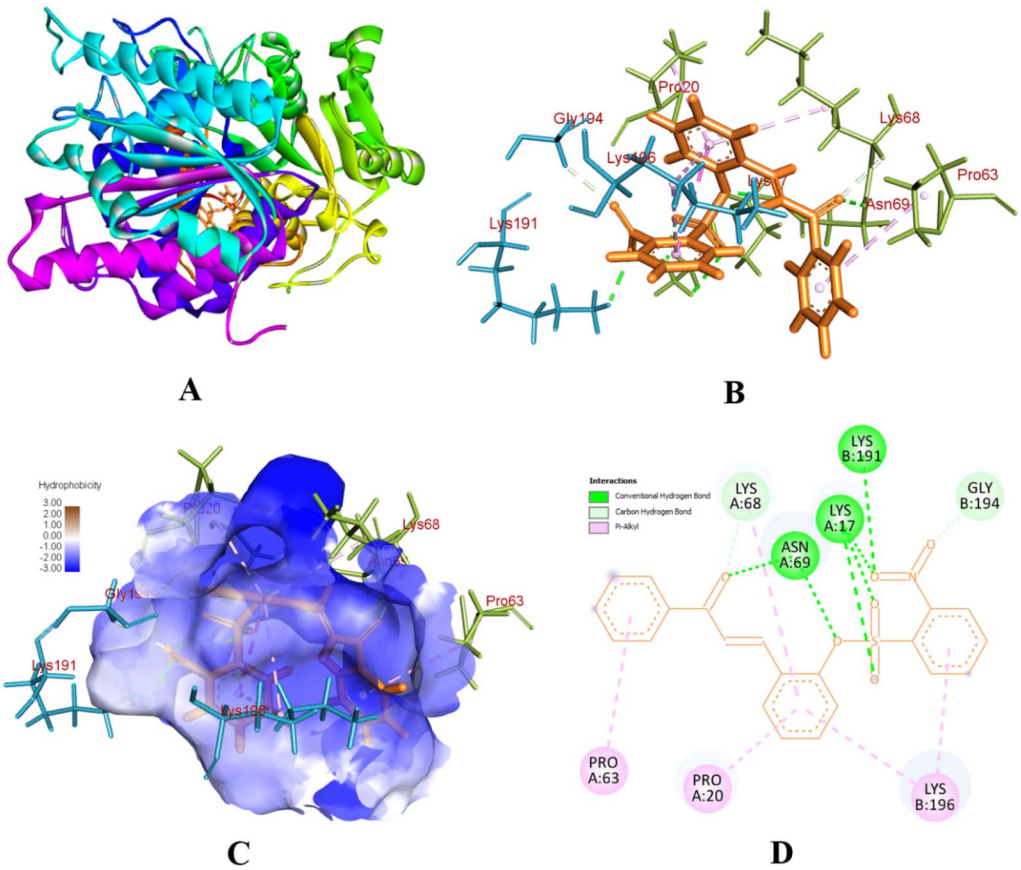

Fig. 5 Interaction of 2ZVA protein with compound 7 (A) structure of protein (B) protein–ligand interaction (C) hydrophobic interaction (D) 2D diagram of ligand.

these hydrophobic contacts are facilitated is the aromatic rings of the chalcone scaffold. Fig. 6 shows the docking pose and interaction diagram of the compound **5**-1SMD protein in three dimensions, with the positional orientation of the ligand in the enzyme active site clearly shown. In comparison, Fig. S3 in the SI file shows the interaction pattern of the reference drug acarbose with the same protein. Even though acarbose establishes numerous hydrogen bonds because of its polyhydroxylated structure, compound **5** exhibits intense hydrophobic reactions that also facilitate stable binding in the active cavity.

3.4.2.2 Interaction with 5U3A protein. Docking simulations of the synthesized derivatives against the pancreatic 5U3A protein were also conducted to provide further evidence regarding the inhibitory potential of the compounds. The results of the docking are summarized in Table S4 in the SI file. Like the findings made on the 1SMD protein, compound **5** possessed good binding affinity to the 5U3A protein. It was observed in the interaction analysis that the ligand establishes stabilizing contacts with enzyme residues found within the catalytic region of the enzyme. The hydrophobic interactions with the aromatic and nonpolar residues also have a major role in stability of the ligand in the binding pocket.

Fig. 7 shows the graphical depiction of the docking contacts between compound **5** and the 5U3A protein: the three-dimensional binding conformation, hydrophobic effects and the interaction diagram in 2D format. Fig. S4 in SI file demonstrates the docking interaction of the reference inhibitor acarbose with 5U3A protein to aid in a comparative framework of assessing the profile of interaction between the synthesized compounds. On the whole, the docking results indicate that compound **5** has positive binding affinities with both of the α-amylase proteins, and therefore, demonstrates that compound **5** has the potential to be a viable carbohydrate-digesting enzyme inhibitor.

3.4.3. General impression of docking study. The molecular docking experiment on Molegro Virtual Docker has shown that meaningful interactions existed between the synthesized chalcone sulfonate ester derivatives and the chosen enzyme targets to urea and carbohydrate metabolism. The most promising binding interactions with urease-related proteins (1OTH and 2ZAV) were observed in compound **7**, which has several hydrogen bonds with the following residues (ARG270, ASN198, HIS202, and SER267) as well as hydrophobic interactions (ASP165 and LEU166). Moreover, compound **5** exhibited the highest level of interaction with the 5U3A and 1SMD proteins (α-amylase) mainly due to the extensive π–π interactions and hydrophobic interactions of the compounds with the residues, namely, TYR62, TRP58, TRP59, HIS201, HIS305, and ILE235. These results indicate that compounds **5** and **7** can be taken as

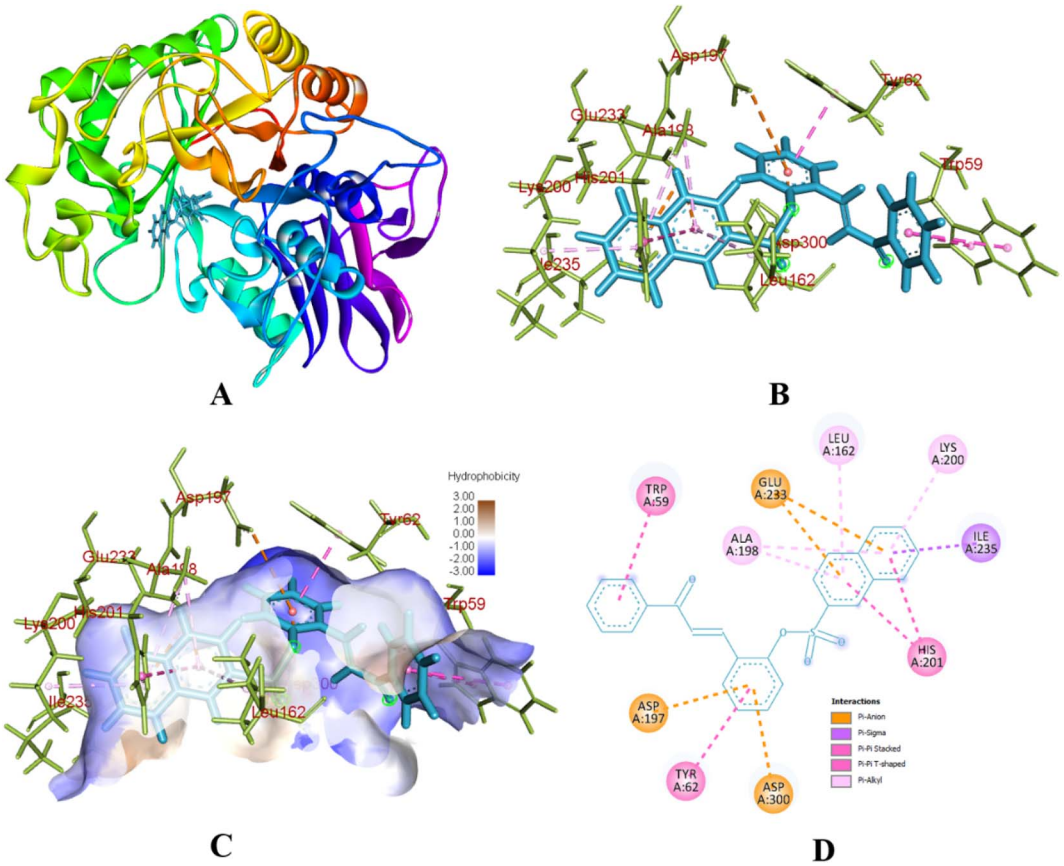

Fig. 6 Interaction of 1SMD protein with compound **5** (A) structure of protein (B) protein–ligand interaction (C) hydrophobic interaction (D) 2D diagram of ligand.

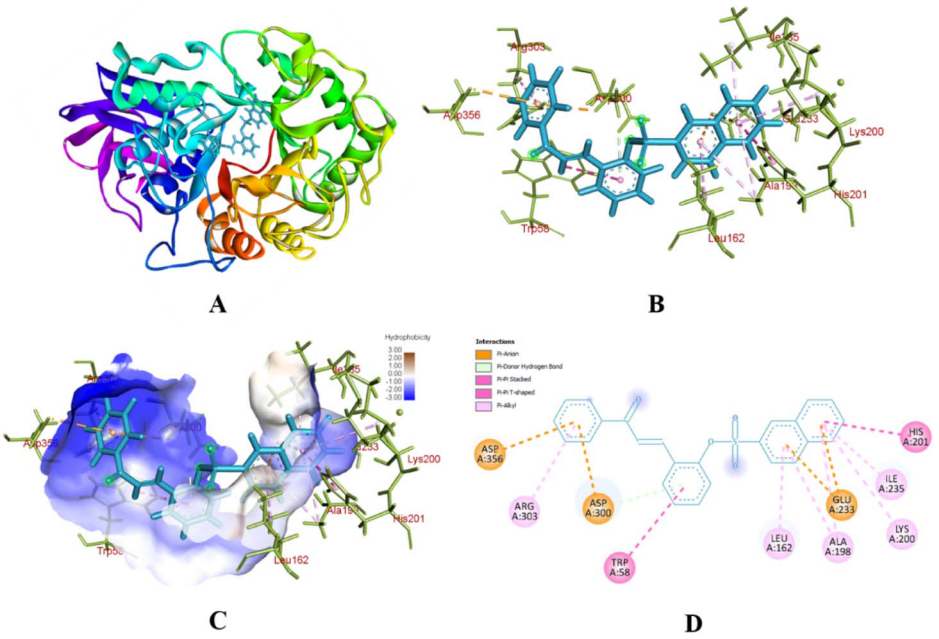

Fig. 7 Interaction of 5U3A protein with compound 5 (A) structure of protein (B) protein–ligand interaction (C) hydrophobic interaction (D) 2D diagram of ligand.

potential lead molecules, because they have high docking scores and stable interaction with the active sites of the corresponding target enzymes. Due to the consistent results of the docking study, the experimental inhibitory activity, and the valuable structural insights that can be obtained, the study will be useful in the optimization and development of the chalcone-based enzyme inhibitors.

3.4.4. Validation of docking. The redocking study was done to establish the validity of the docking methodology used in the current study. The natural co-crystallized ligands of the chosen protein structures 1OTH, 2ZAV, 1SMD and 5U3A were initially stripped off and re-docked into the binding cavities of the respective proteins with Molegro Virtual Docker. Accuracy of the docking protocol was measured as the root mean square deviation (RMSD) between the docked ligand pose and the obtained crystallographic ligand conformation. The value of RMSD gives a measure of how similar the two ligand structures are, but the smaller the RMSD values, the more the structures agree with the experimental binding orientation. The RMSD of the redocked ligands in the proteins 1OTH and 2ZAV (urease proteins) and 1SMD and 5U3A (α-amylase proteins) were observed to be in an acceptable range of less than 2.0 Å. Such values have shown that the docking procedure effectively recapitulated the experimentally determined ligand binding affinity poses at the active sites of the chosen proteins.

Fig. 8 shows the superimposition of the redocked ligand and crystallographic ligand conformations. This figure clearly shows that there is a great overlap between the two structures, which means that there is less deviation between the experimental and predicted binding orientation. The low RMSD values and similar close structural overlap of the docked and crystallographic ligand confirm that the Molegro Virtual Docker docking protocol employed in this study is an effective and reliable one that can predict accurately the ligand binding orientations within the active site of the target proteins. Thus, the docking values achieved on the synthesized chalcone sulfonate ester derivatives with urease (1OTH and 2ZAV) and α-amylase (1SMD and 5U3A) can be deemed as valid and structurally sound to deduce the mechanism of interactions of the studied compounds.

3.4.5. MD simulation study. The simulation of stability and dynamics of docked complexes of chalcone sulfonate esters and their respective target proteins was performed using the method of MD simulations. MD simulation helps to supply valuable data on the structural stability of protein–ligand complexes in a physiological environment over time. The ligands, compound 7-2ZAV and compound 5-5U3A, in this study were subjected to evaluation of the dynamic stability of the complexes over a simulation time of 25 ns. A number of structural parameters, such as RMSD, RMSF, radius of gyration, hydrogen bonding, and SASA were examined in order to ascertain the stability and conformational alterations of the complexes. The simulation findings are described in Fig. 9 and 10.

3.4.5.1 RMSD analysis. An important parameter that is used to measure the extent of stability of a protein–ligand complex in the MD simulation is the root mean square deviation (RMSD). The values of RMSD show the extent of the deviation of the structure from its original conformation over time in the simulation. The profile of RMSD values of the compound 7-2ZAV complex, as depicted in Fig. 9A, indicated a rise at the beginning of the nanoseconds as the system acclimatized to the simulated environment. Following this equilibration step, the values of the RMSD have reached a value of stability and oscillated within a reasonable range, which proves that the complex

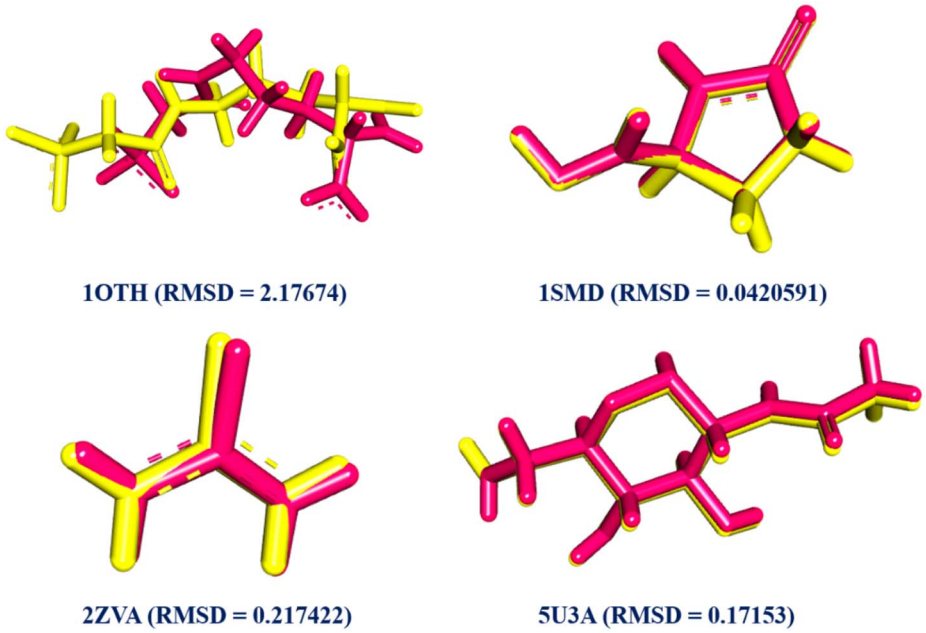

Fig. 8 Superimposable structures of redocking proteins.

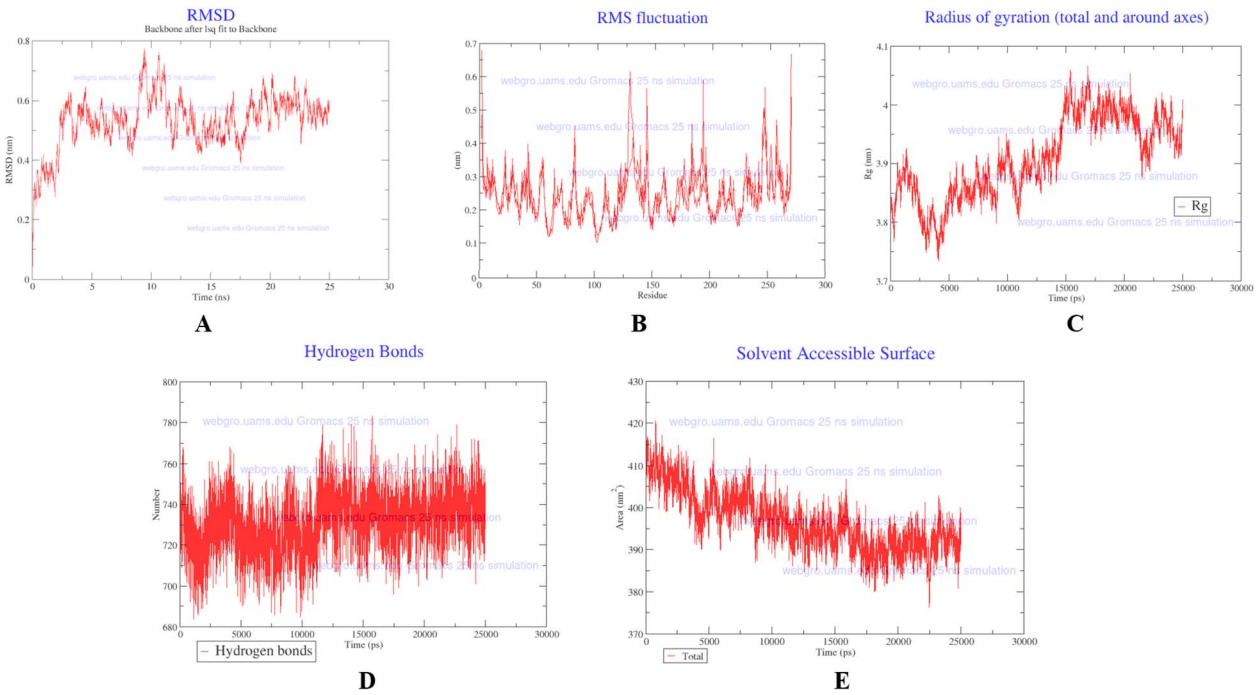

Fig. 9 MD simulation of a complex of compound **7** with 2ZAV (A) RMSD (root mean square deviation) (B) RMSF (root mean square fluctuation) (C) radius of gyration (D) hydrogen bonds (E) SASA (solvent accessible surface area).

had retained its structural integrity within the timeframe of the simulation. The small deviations are indicative of the fact that the ligand was very tightly bound to the active site of the protein. Fig. 10A of the RMSD plot of the **5**-5U3A complex showed a similar trend. RMSD had initially risen as a result of structural relaxation but reached a steady level. The fact that the values of the RMSD stabilized during the rest of the simulation period suggests that the complex was in the same conformation, and that the interaction between the ligand did not cause significant structural changes in the protein. In general, the RMSD findings indicate the dynamic stability of the two complexes at 25 ns of the simulation time.

3.4.5.2 RMSF analysis. Root mean square fluctuation (RMSF) can be used to give information about the flexibility of

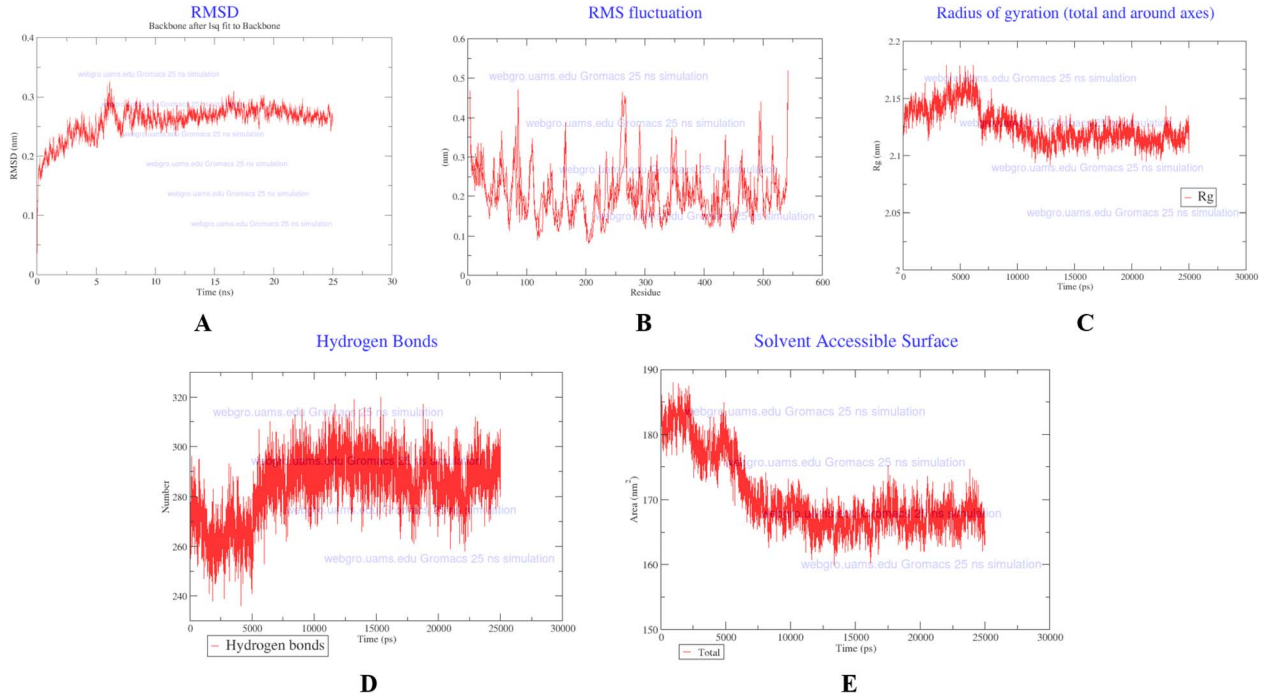

Fig. 10 MD simulation of a complex of compound **5** with 5U3A (A) RMSD (root mean square deviation) (B) RMSF (root mean square fluctuation) (C) radius of gyration (D) hydrogen bonds (E) SASA (solvent accessible surface area).

individual amino acid residues in the protein at the time of the simulation. RMSF profile of the compound 7-2ZAV complex in Fig. 9B indicates that the majority of the residues had fairly low fluctuations, which implies that there were not much mobility and the structure of the protein remained stable throughout the course of the simulation. The terminal regions and loop areas of the protein were found to be more fluctuated than the rest of the protein, which is common as these areas tend to be more flexible than the structural core of the protein.

In the case of the compound **5**-5U3A complex, Fig. 10B of the RMSF graph depicted a similar pattern, and most residues had low values of fluctuations. The residues in the proximity of the binding pocket had minimal variations, which indicates that the binding of the ligand helped to stabilize the active site region. These results mean that the binding of the ligands did not destabilize the protein structure significantly and the complexes retained stable dynamics of the residues during the simulation.

3.4.5.3 Radius of gyration (R_g). The radius of gyration (R_g) is used to show the compactness of the protein structure during the simulation. A constant R_g value usually means that the protein does not change its structural compactness and does not change significantly in its conformational form. Fig. 9C demonstrates that the compound 7-2ZAV complex had rather stable values of the R_g during the course of the simulation, which means that the protein retained the same degree of compactness. It only saw slight variations, and this is normal in the course of dynamic simulations. Equally, the R_g profile of the compound **5**-5U3A complex, as illustrated in Fig. 10C, depicted a steady behavior with slight changes across the simulation. These values of R_g are consistent, which implies that the protein structure was not unfolded or unstable by the ligand binding.

3.4.5.4 Hydrogen bond analysis. Hydrogen bonds are important in stabilizing the protein–ligand interactions. The simulation of hydrogen bond formation between the protein and the ligand gives an idea of the binding reaction strength and stability. The analysis of hydrogen bonds of the compound 7-2ZAV complex, as depicted in Fig. 9D, indicated that a persistent hydrogen bond existed during the duration of the simulation. The number of hydrogen bonds had minor changes, though the interactions were mostly preserved, which implied that the ligand was not washed out of the active site. In the case of the compound **5**-5U3A complex, the hydrogen bond profile, as indicated in Fig. 10D, revealed similar hydrogen bond interactions within the simulation period. The existence of hydrogen bonds throughout the interaction with the ligand assists in the stability of the interaction with the protein and the additional demonstration of the high affinity of the binding proposed by the docking outcomes.

3.4.5.5 Solvency-accessible surface area (SASA). The surface area of the protein that is available to solvent molecules is termed the solvent accessible surface area (SASA). The alteration of SASA values may reflect the structural reorganization or a conformational alteration of the protein. Fig. 9E, which is a SASA profiling of compound 7-2ZAV complex, indicated that values were quite constant with some slight fluctuations throughout the simulation. This is a pointer that the structure of the protein did not experience significant unfolding throughout the simulation. On the same note, the analysis using SASA on the compound **5**-5U3A complex, illustrated in

Fig. 10E, revealed that the values were stable throughout the simulation period. The minor changes that have been witnessed are characteristic of normal protein breathing movements and are not indicative of significant structural instability.

3.5. Density functional theory

The electronic structure, stability, and chemical reactivity of chalcone sulfonate ester derivatives (**5** and **7**) were determined through DFT calculations as compared to the reference inhibitors acarbose and thiourea. The calculations were all done using Gaussian 09 at a B3LYP/6-311G level of theory. To assess the stability and reactivity of the molecules, several electronic parameters were obtained, such as dipole moment, HOMO–LUMO energies, energy gap (ΔE), and global reactivity parameters. The electronic parameters have been calculated and optimized in Table S5 in the SI file, and the frontier molecular orbitals, molecular electrostatic potential maps, and optimized molecular structures are shown in Fig. 11–13.

3.5.1. Optimized molecular structures. All the studied molecules have been optimized using the full geometry optimization of theory at the level of B3LYP/6-311G. The optimized confirmations are given in Fig. 11. The chalcone derivatives have fairly planar structures since the aromatic rings and the unsaturated carbonyl group (amine group) are extensively π-conjugated. This conjugated structure facilitates the delocalization of electrons across the molecular structure, which leads to a higher level of structural stability. The total electronic energies of the compounds calculated show some slight differences. Table S5 in the SI file indicates that compound **7** has a lower total energy (−1713.182469 hartree) than compound **5** (−1662.361236 hartree) and consequently, compound **7** has a relatively greater thermodynamic stability. Different molecules are used to obtain these reference molecules since they have varying energy values due to their size and structure. Values of dipole moments give information on the degree of polarity and the possibilities of intermolecular interactions of the molecules. Acarbose is more polar in nature and can easily interact with the polar environment, as indicated by its highest dipole moment (9.20 debye) among the compounds studied. On the contrary, compound **5** has a dipole moment of 6.71 debye, with a slightly lower measurement of 5.57 debye in compound **7**. Their moderate dipole moments are believed to favor drug-like behavior because they are able to maintain the balance between solubility and membrane permeability, and still enable effective interactions with the biological targets.

3.5.2. Frontier molecular orbital (FMO) analysis. FMO analysis is useful in giving a clue to the reactivity and ability to interact with other molecules in a system through electronics. The Highest Occupied Molecular Orbital (HOMO) is the ability of a molecule to donate electrons, and the Lowest Unoccupied Molecular Orbital (LUMO) is the ability to accept electrons. The spatial distribution of these orbitals has been given in Fig. 12, and their corresponding energies have been tabulated in Table S5 in the SI file. The HOMO of acarbose, thiourea, compound **5**, and compound **7** were calculated to be −0.21573 hartree, −0.21029 hartree, −0.24412 hartree, and −0.24634 hartree, respectively. The observed slightly lower HOMO energies of the

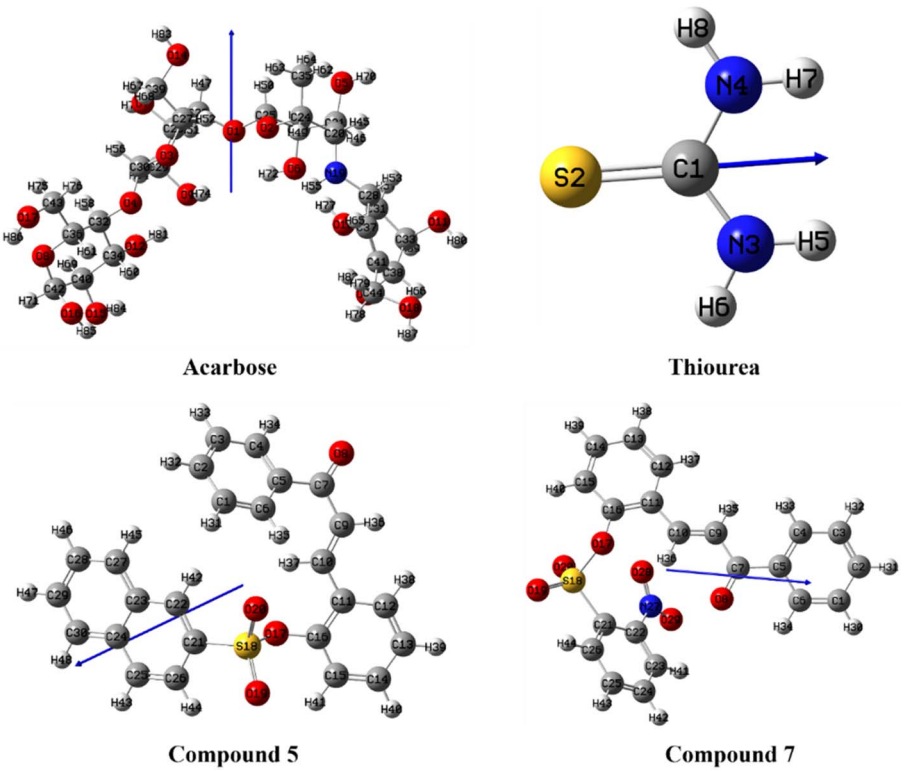

Fig. 11 Optimized structure of lead compounds and reference drugs acarbose and thiourea.

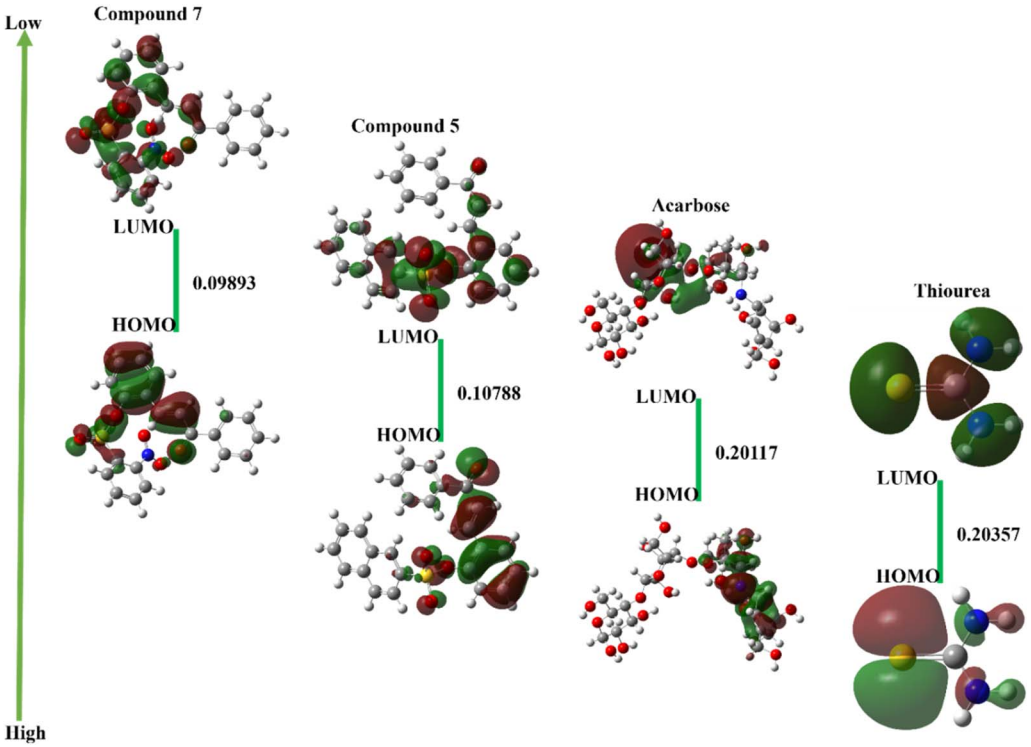

Fig. 12 HOMO, LUMO, and energy gap of lead compounds and reference drugs acarbose and thiourea.

chalcone derivatives indicate that the compounds are more stable in electrons compared to the reference compounds, since more energy is needed to remove an electron from the compounds. Similarly, the chalcone derivatives have lower LUMO energies than the reference molecules. Compound **7** is the one with the lowest LUMO energy (−0.14741 hartree), then compound **5** (−0.13624 hartree), which means an increased electron-accepting capacity. Another valuable parameter to consider in measuring the stability of a molecule and its chemical reactivity is the HOMO–LUMO energy gap (ΔE). The smaller the energy gaps are, the more chemical reactivity and potential interaction. The energy gaps that have been computed are 0.20117 hartree for acarbose, 0.20357 hartree for thiourea, 0.10788 hartree for compound **5**, and 0.09893 hartree for compound **7**. These findings make it clear that compound **7** has the smallest energy gap, followed by compound **5**, which is the indication of greater reactivity than the reference compounds. The higher the reactivity, the greater the biological activity is usually related to this, and again, the higher docking interactions were seen with these chalcone derivatives.

3.5.3. Global reactivity parameters. FMO-derived global reactivity descriptors have valuable information on the chemical reactivity, stability, and electron transfer properties of molecular systems. The global descriptors calculated, such as ionization potential (I), electron affinity (A), chemical potential (μ), electronegativity (χ), chemical hardness (η), chemical softness (S), electrophilicity index (ω), nucleophilicity index (N), among other electronic charges, are listed in Table S5 in the SI file. Ionization potential is the energy needed to lose an electron in a molecule, and thus it is linked to molecular stability to oxidation. An increase in the ionization potential values is usually a sign of greater resistance to the removal of electrons. In this study, compound **7** (0.24634 hartree) and compound **5** (0.24412 hartree) have slightly higher ionization potential than the reference compounds acarbose (0.21573 hartree) and thiourea (0.21029 hartree), indicating the possibility of increased electronic stability of the chalcone derivatives.

Electron affinity is a property that defines the capacity of a molecule to take in an electron. The highest electron affinity of the studied molecules is compound **7** (0.14741 hartree), and then there is compound **5** (0.13624 Hartree). These values suggest that the chalcone derivatives are more likely to accept electrons during intermolecular interactions and thus they may show a higher binding affinity with biological targets. The chemical hardness (η) and chemical softness (S) are the terms used to characterize the resistance and the flexibility of a molecule to transfer charges. Lower values of hardness and higher values of softness are normally associated with greater chemical reactivity and flexibility of the molecules. Compounds **5** and **7** are found to be less hard than the reference molecules (0.05394 hartree and 0.04947 hartree, respectively), and the softness values of **5** and **7** are significantly larger (18.54 and 20.22, respectively). In contrast, acarbose and thiourea have relatively lower softness values (9.94 and 9.83). Such findings suggest that the chalcone derivatives are more flexible and have a higher potential in binding the biological receptors.

Chemical potential (μ) is the escaping value of electrons out of a molecule and the potential to engage in an electron transfer

reaction. Compound 7 has the highest chemical potential (0.19688 hartree), then compound 5 (0.19018 hartree), meaning it has the most propensity to engage in charge transfer interactions in the process of molecular recognition. Electrophilicity index is the measure of the ability of a molecule to accept electrons. Compound 7 has the greatest electrophilicity value (0.3918 hartree) and 5 (0.3353 hartree), which is larger than that of the reference compounds. The behavior is expected by their frontier orbital properties, with especially low LUMO energies that are conducive to electron acceptance. Also, the extra values of the electronic charges of the chalcone derivatives (−3.53 in case of compound 5 and −3.98 in case of compound 7) are more negative than the ones of reference molecules, which confirms their greater acceptance of electrons and higher values of charge transfer interaction. Therefore, global reactivity parameters reveal that compounds 5 and 7 have a smaller HOMO–LUMO energy gap, greater softness, and electrophilic nature than the reference compounds. Compound 7 has the most favorable electronic properties, indicating increased chemical reactivity and improved possibilities to interact with the biological target.

3.5.4. Molecular electrostatic potential (MEP) analysis. MEP mapping can be very useful in obtaining the charge distribution information in a molecule and in identifying areas prone to electrophilic or nucleophilic attack. Fig. 13 gives the MEP surfaces of the optimized structures. The electrostatic potential is indicated by a color scale in these maps; red is used to denote the parts of the map that have high electron density, blue is used to denote the parts of the map that lack electrons, and green is used to denote the parts of the map that have neutral potential. In the case of the chalcone sulfonate ester derivatives, the regions of negative electrostatic potential are mainly localized in the oxygen atom of the carbonyl and sulfonate groups. These sites are shown in red on the MEP surface and are sites rich in electrons, which may be involved in electrophilic reactions with amino acid residues or a hydrogen bond in biological systems. On the other hand, positive electrostatic potential areas (blue) are primarily located around hydrogen atoms and some aromatic areas, as well as the possibility of nucleophilic interaction points. Electrostatic distribution is in agreement with the patterns of interactions found in molecular docking and molecular dynamics modeling of the interaction; hydrogen bonds and electrostatic interactions have a significant part in the stabilization of protein–ligand complexes.

3.5.5. ELF and LOL analysis. To explore further the electron distribution and bonding features of the chalcone sulfonate derivatives in the ester form, Electron Localization Function (ELF) and Localized Orbital Locator (LOL) calculations were carried out. These descriptors in real space give a clue to the localization of electrons, bonding interaction, lone pair, and

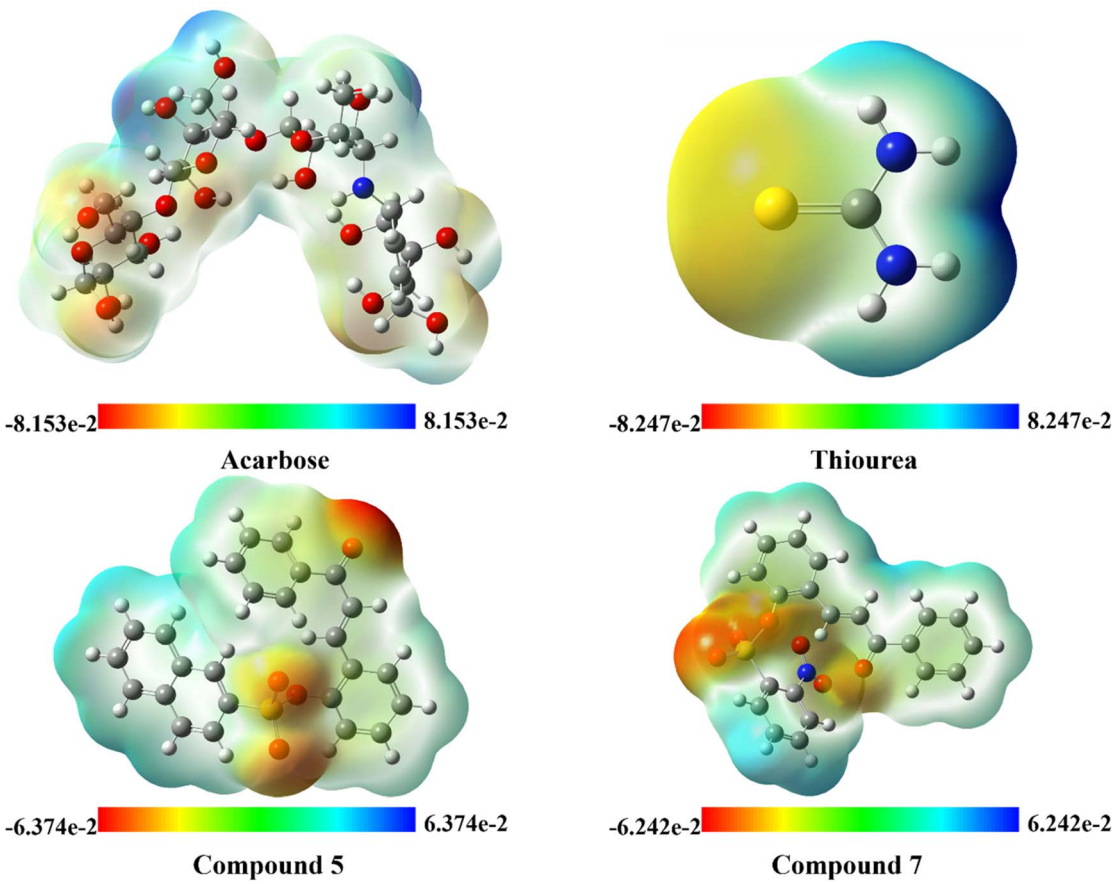

Fig. 13 MEP structure and scale of lead compounds and reference drugs acarbose and thiourea.

delocalization of π electrons in molecular systems. Fig. 14 and 15 give the corresponding ELF and LOL isosurfaces obtained using DFT wavefunction data. The ELF maps show the localized and delocalized electron density distribution within the molecular structure. Those regions that are high in ELF (almost reaching 1.0) are those that would be represented by red or yellow colors and are highly localized electrons, including bonding pairs and lone pairs. Regions with smaller ELF values (green or blue), in contrast, have delocalized electron density. There is great evidence of electron localization around oxygen atoms of the sulfonate groups that can be seen in the ELF visualization, which makes sense given the existence of lone pair electrons. These areas are represented by bright red spots, which validate the high density of electrons of these hetero atoms. A high level of localization is also observed in the carbonyl (C═O) and (C–O) bonds, which indicates that there were strong covalent bonding interactions. In the meantime, it is possible that the aromatic rings in the chalcone structure have moderate levels of electron localization on the ring structures, which implies that there is delocalized π-electron conjugation, resulting in general molecular stability. These observations are also supported by the LOL analysis. Large LOL values are associated with localized bonding orbitals and lone pairs, whereas smaller ones are associated with electron delocalization. The LOL contour plots show high orbital localization of the oxygen atom of the sulfonate and carbonyl groups, which are significant in the intermolecular interactions and the donation of electrons. Furthermore, moderate orbital localization of the aromatic rings is an indication that there is a presence of long π-conjugation in the backbone of chalcone.

3.5.6. RDG and NCI analysis. Multiwfn program was used to perform Reduced Density Gradient (RDG) and Non-Covalent Interaction (NCI) analyses to study weak intermolecular and intramolecular interactions. Fig. 16 and 17 show the RDG scatter plots and the isosurface of NCI. The RDG scatter plot is used to show the correlation between the decreasing density gradient and the electron density that is sign(λ_2)ρ, so that various forms of non-covalent interactions can be identified. Attractive interactions, hydrogen bonding, and electrostatic are associated with negative values of sign(λ_2)ρ, attractive but weakly attractive van der Waals are associated with zero values, and steric repulsion with positive values. A number of spikes of sign(λ_2)ρ of the RDG plots show that there were weak van der Waals interactions in the molecular framework. They are primarily involved in reactions between aromatic rings and other functional groups that are adjacent and provide structural stabilization. The negative region also has some small peaks, which indicate the existence of weak hydrogen bonds between the oxygen atom of the sulfonate groups and the surrounding hydrogen atom. Such interactions are also visualized by NCI isosurface analysis. The blue regions in the NCI plots are strong attractive forces like hydrogen bonds, the green ones are weak van der Waals forces, and the red ones are steric repulsions. The NCI isosurfaces reveal a lot of green areas dispersing around the

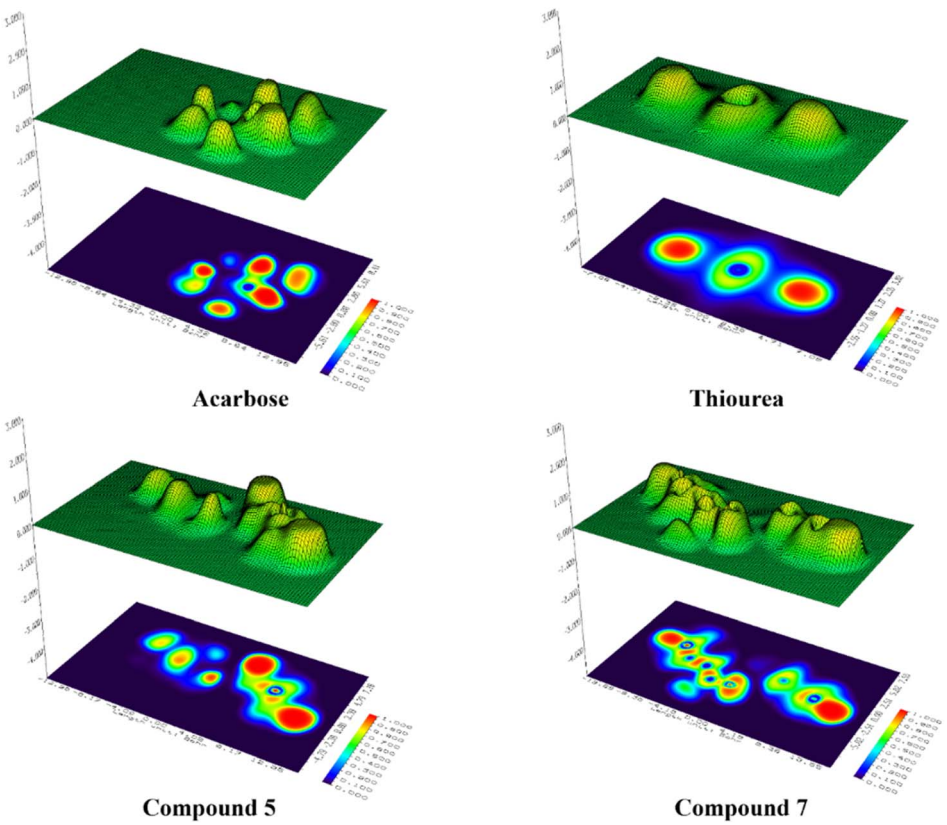

Fig. 14 ELF plots of lead compounds and reference drugs acarbose and thiourea.

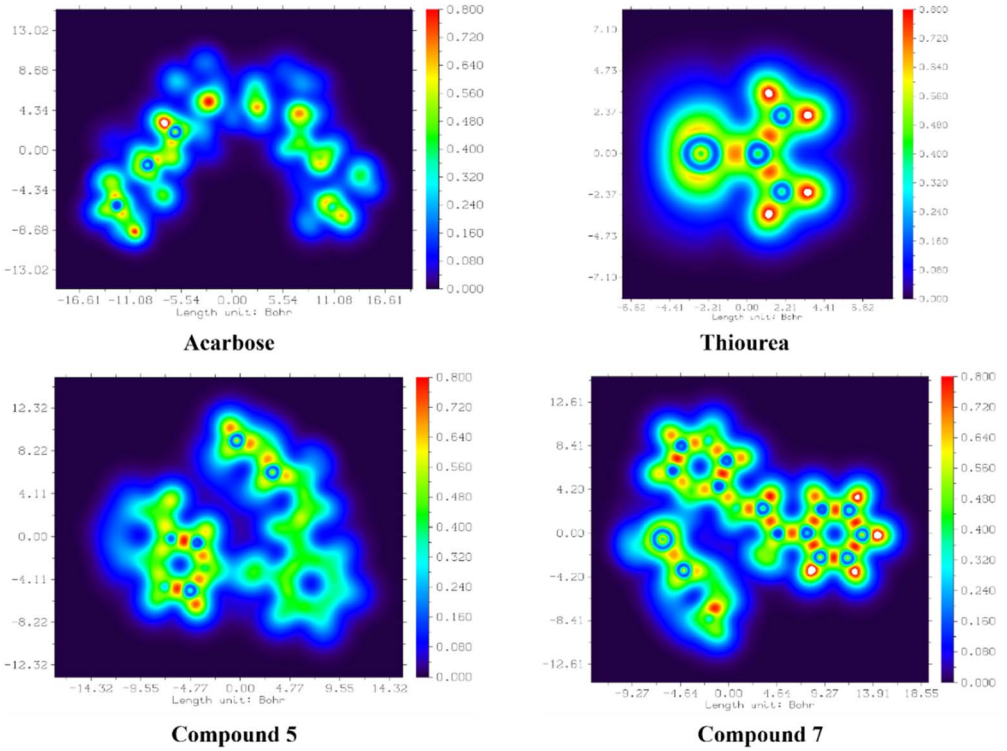

Fig. 15 LOL plots of lead compounds and reference drugs acarbose and thiourea.

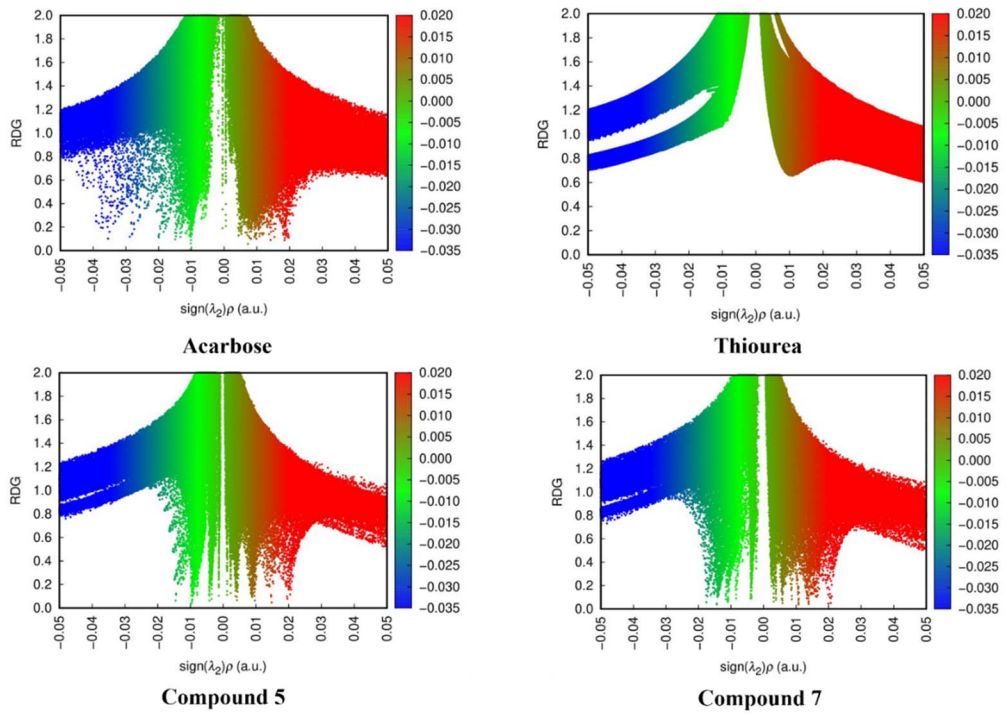

Fig. 16 RDG plots of lead compounds and reference drugs acarbose and thiourea.

aromatic rings and among the functional groups adjacent to each other, and it proves the existence of weak van der Waals interactions stabilizing the molecular geometry. The fact that there are small regions of blue color seen around the oxygen atom of the sulfonate and carbonyl groups implies that there are weak attractive forces that can cause the stabilization of the molecule and binding to biological targets. The presence of red

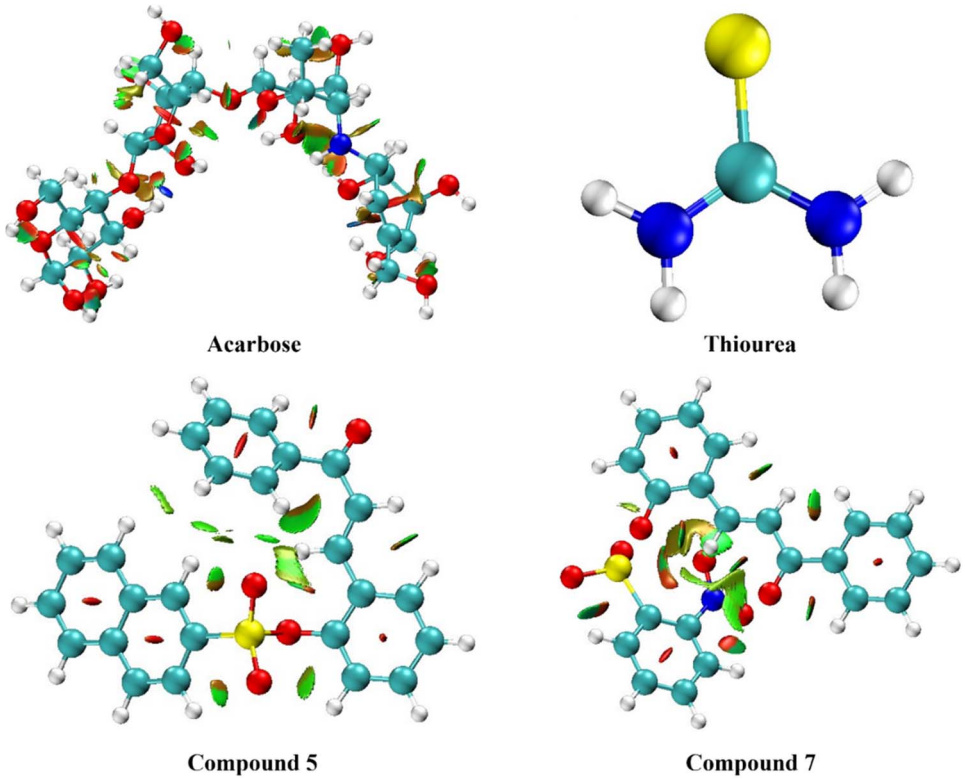

Fig. 17 NCI plots of lead compounds and reference drugs acarbose and thiourea.

regions in places of close atomic proximity indicates steric repulsion in some of the parts of the molecular structure.

4. Conclusions

In this study, a series of chalcone–sulfonate ester derivatives (**1**–**7**) were successfully synthesized and evaluated for their inhibitory potential against urease and α-amylase enzymes. The *in vitro* enzymatic assays demonstrated that the synthesized compounds possess promising inhibitory activities, with IC_{50} values ranging from 6.5–19.5 μM for urease and 5.2–27.5 μM for α-amylase. Among the evaluated derivatives, compounds **5** and **7** emerged as the most potent inhibitors. Compound **7** exhibited the strongest urease inhibition, surpassing the reference inhibitor thiourea, whereas compound **5** showed the highest dual inhibitory activity against both enzymes, including superior potency against α-amylase compared with acarbose. The SAR analysis has demonstrated the critical role of the chemical nature of substituents on the sulfonate aromatic ring to regulate biological activity. A few derivatives were expected to have a high gastrointestinal absorption and pass significant drug-likeness filters. In particular, compounds **3** and **7** proved to have balanced lipophilicity, encouraging predictions of absorption, and limited the number of violations of essential sets of rules, which highlights their potential as drug-like candidates. The molecular docking experiments provided additional evidence on the binding of the synthesized derivatives to enzymes, urease and α-amylase. Compound **7** has a high binding affinity toward proteins of urease 1OTH and 2ZAV, which was mediated by multiple hydrogen bonds and hydrophobic interactions between catalytic residues. In contrast, compound **5** interacted well with the proteins of 1SMD and 5U3A amylases and with both of them largely due to the presence of π–π screenings and hydrophobic interactions. The reliability of the computational methodology was validated by redocking experiments that eventually provided RMSD values that were less than 2.0 A. The most valid protein–ligand complexes retained the stability of interaction during a 25 ns MD simulation. DFT calculations were important in giving valuable insight into the electronic properties and chemical reactivity of the main compounds. Compounds **5** and **7** were found to be more chemically soft, electrophilic, and less HOMO–LUMO energy gaps than the reference inhibitors, which showed lower chemical reactivity and lower biological binding affinity. Accordingly, compounds **5** and **7** appear as viable lead molecules that should be further refined structurally and eventually tested biologically. Subsequent research involving mechanistic analysis, toxicity, and *in vivo* analysis could further enhance *in vitro* studies of these derivatives as therapeutic agents for disorders related to urease activity and carbohydrate metabolism.

Author contributions

Zobia Noreen: experimental work performance; Amina Sadiq: supervision, investigation and formal analysis; Nafeesa Naeem: data analysis and collection, first-and final draft preparation, visualization and validation; Usama Raza: computational analysis; Ishtiaq Ahmed: performed NMR and mass analyses; Samar

Y. Al Nami: investigation, formal analysis and funding acquisition; Aisha Hossan: investigation, formal analysis and funding acquisition; Magdi E. A. Zaki: investigation, formal analysis and funding acquisition; Ehsan Ullah Mughal: main idea, reviewing and editing, visualization and validation, final writing the manuscript.

Conflicts of interest

Authors have no conflicts of interest to declare.

Data availability

All the data is provided in the manuscript and supplementary information (SI) file. Supplementary information is available. See DOI: https://doi.org/10.1039/d6ra02588a.

Acknowledgements

The authors would like to thank the ORIC Department of Government College Women University Sialkot for providing the research grant under the ORIC Internal Research Grant Program.

References

1 N. A. Elkanzi, H. Hrichi, R. A. Alolayan, W. Derafa, F. M. Zahou and R. B. Bakr, *ACS Omega*, 2022, **7**, 27769–27786.
2 M. A. Shalaby, S. A. Rizk and A. M. Fahim, *Org. Biomol. Chem.*, 2023, **21**, 5317–5346.
3 A. Farzaliyeva, H. Şenol, P. Taslimi, F. Çakır, V. Farzaliyev, N. Sadeghian, I. Mamedov, A. Sujayev, A. Maharramov and S. Alwasel, *J. Mol. Struct.*, 2025, **1321**, 140197.
4 D. Osmaniye, B. M. N. Sağlık, N. Khalilova, S. Levent, G. Bayazıt, U. D. Gul, Y. Ozkay and Z. A. Kaplancıklı, *ACS Omega*, 2023, **8**, 6669–6678.
5 M. F. Mohamed, I. M. Salem, A. Fouad, R. M. Allam, W. A. Fadaly, M. T. Nemr, S. Y. Ewieda, T. S. Ibrahim, N. A. Ibrahim and M. A. Abou-Salim, *Bioorg. Chem.*, 2025, **163**, 108694.
6 A. M. Abd El-Hameed, A. H. Lotfallah, M. T. Nemr, H. K. Abdelhady, H. H. Haredy, A. M. Sayed, M. F. Mohamed, D. E. Elsayed Abouzed and W. A. Fadaly, *Future Med. Chem.*, 2025, **17**, 1849–1865.
7 W. Mi, Y. Xia and Y. Bian, *Inflammation Res.*, 2019, **68**, 275–284.
8 H. Şenol, M. Ghaffari-Moghaddam, G. Ö. A. Toraman and U. Güller, *J. Mol. Struct.*, 2024, **1295**, 136804.
9 O. A. Dar, L. Luo and H. Shao, in *Chalcones and Their Derivatives*, Elsevier, 2026, pp. 125–148.
10 G. George, V. P. Koyiparambath, S. Sukumaran, A. S. Nair, L. K. Pappachan, A. G. Al-Sehemi, H. Kim and B. Mathew, *Int. J. Mol. Sci.*, 2022, **23**, 3121.
11 F.-u. Hassan, C. Liu, M. Mehboob, R. M. Bilal, M. A. Arain, F. Siddique, F. Chen, Y. Li, J. Zhang and P. Shi, *Front. Immunol.*, 2023, **14**, 1285052.
12 A. Korkmaz and E. Bursal, *J. Mol. Struct.*, 2025, **1332**, 141638.
13 H. Aslan, F. Yetişsin, A. Korkmaz and E. Bursal, *ChemistrySelect*, 2024, **9**, e202400053.
14 A. Korkmaz, *J. Mol. Struct.*, 2023, **1286**, 135597.
15 A. Korkmaz and E. Bursal, *Chem. Biodiversity*, 2022, **19**, e202200140.
16 X. Chen, C. Chen, X. Tian, L. He, E. Zuo, P. Liu, Y. Xue, J. Yang, C. Chen and X. Lv, *Talanta*, 2024, **266**, 125052.
17 X. Chen, C. Chen, C. Ma, W. Kang, J. Wu and X. Fu, *Food Sci. Hum. Wellness*, 2025, **14**, 9250007.
18 A. Günsel, C. C. Karanlık, P. Taslimi, H. Günsel, T. Taskin-Tok, A. T. Bilgiçli, E. M. Özden, İ. Gülçin, A. Erdoğmuş and M. N. Yarasir, *Photochem. Photobiol. Sci.*, 2026, 1–14.
19 E. Bursal, A. Korkmaz and F. Yetişsin, *ChemistrySelect*, 2025, **10**, e202500128.
20 X. Chen, C. Chen and X. Fu, *Food Funct.*, 2022, **13**, 10121–10133.
21 E. Agbo, B. Maluleke, S. Gildenhuys, T. Leboho and W. Nxumalo, *Sci. Rep.*, 2025, **15**, 36575.
22 T. Guo, R. Xia, M. Chen, J. He, S. Su, L. Liu, X. Li and W. Xue, *RSC Adv.*, 2019, **9**, 24942–24950.
23 S. Sepehri and M. Khedmati, *Arch. Pharm.*, 2023, **356**, 2300252.
24 M. M. Al-Rooqi, E. U. Mughal, Q. A. Raja, E. M. Hussein, N. Naeem, A. Sadiq, B. H. Asghar, Z. Moussa and S. A. Ahmed, *RSC Adv.*, 2023, **13**, 3210–3233.
25 N. Naeem, S. Zaib, E. U. Mughal, G. A. Othman, A. Sadiq and N. Rana, *Future Med. Chem.*, 2025, **17**, 929–941.
26 S. Gharge and S. G. Alegaon, *Chem. Biodiversity*, 2024, **21**, e202301738.
27 W. A. Fadaly, A. Elshewy, M. T. Nemr, K. Abdou, A. M. Sayed and N. M. Kahk, *Bioorg. Chem.*, 2024, **152**, 107760.
28 M. Padmapriya, S. S. Hakkimane and S. L. Gaonkar, *Discover Appl. Sci.*, 2025, **7**, 208.
29 G. P. Sadawarte, J. D. Rajput, A. D. Kale and V. B. Jagrut, *J. Chem. Rev.*, 2024, **6**, 331–352.
30 D. Kısa, E. Koç, K. S. Baş Topcu and R. İmamoğlu, *J. Biomol. Struct. Dyn.*, 2024, **42**, 12144–12153.
31 M. A. Shalaby, A. M. Fahim and S. A. Rizk, *Sci. Rep.*, 2023, **13**, 4999.
32 M. A. Mostafa, M. A. Ibrahim and A.-S. Badran, *Synth. Commun.*, 2024, **54**, 1523–1550.
33 M. H. Gailan, M. S. Hussein and G. F. Elmasry, *ChemistrySelect*, 2024, **9**, e202401118.
34 E. U. Mughal, S. Amjid, A. Sadiq, N. Naeem, Y. Nazir, H. Alrafai, A. A. Hassan, S. Y. Al-Nami, A. A. Abdel Hafez and S. W. Ali Shah, *J. Biomol. Struct. Dyn.*, 2024, **42**, 244–260.
35 M. Guerfi, M. Berredjem, A. Dekir, R. Bahadi, S.-E. Djouad, T. O. Sothea, R. Redjemia, B. Belhani and M. Boussaker, *Mol. Diversity*, 2024, **28**, 1023–1038.
36 M. A. Mp, C. P. Somaiya, P. K. Singhal, A. K. Nigam, A. Mukherjee and K. P. Baalann, *Tuijin Jishu*, 2023, **44**, 2023.
37 D. S. Megawati, J. Ekowati and S. Siswodihardjo, *Lett. Drug Des. Discovery*, 2024, **21**, 3913–3922.
38 J. Monga, N. S. Ghosh, S. Kamboj and M. Mukhija, *J. Mol. Chem.*, 2023, **3**, 590.

39 R. Gupta, A. Raza, S. K. Singh, J. Kaur and P. Wadhwa, *Curr. Signal Transduction Ther.*, 2025, **20**, E15743624305290.
40 A. T. Agustin, A. I. Muflihah, A. F. Wijaya, H. Mufidah and J. Riranto, *Int. J. Health Med. Res.*, 2023, **02**, 499–511.
41 A. D. Savitri, H. B. Hidayati, L. Veterini, M. S. Widyaswari, A. R. Muhammad, A. Fairus, M. Q. B. Zulfikar, M. Astri, N. A. Ramasima and D. P. Anggraeni, *Jordan J. Biol. Sci.*, 2023, **16**, 7–12.
42 S. Karakkadparambil Sankaran and A. S. Nair, *J. Biomol. Struct. Dyn.*, 2023, **41**, 6459–6475.
43 M. Hussain, N. Kanwal, A. Jahangir, N. Ali, N. Hanif and O. Ullah, *Front. Chem.*, 2024, **12**, 1493165.
44 K. Gören, E. Çimen, V. Tahiroğlu and Ü. Yıldıko, *Bitlis Eren Univ. J. Sci.*, 2024, **13**, 659–672.
45 N. Karakuş, *Cumhuriyet Sci. J.*, 2024, **45**, 282–290.
46 K. Arulaabaranam, S. Muthu, G. Mani and A. B. Geoffrey, *Heliyon*, 2021, **7**, 1–12.
47 F. Akman, A. Demirpolat, A. S. Kazachenko, A. S. Kazachenko, N. Issaoui and O. Al-Dossary, *Molecules*, 2023, **28**, 2684.